# A comprehensive comparative study of ultrasound-alkaline and thermal-alkaline hydrolysis of duck feather

Nidal del Valle Raydan, Antoine Loquet, Birgit Habenstein, Brice Kauffmann, Bertrand Charrier, Gregory Chatel, Eduardo Robles

Journal of Cleaner Production 467 (2024) 142927

Contents lists available at ScienceDirect

Journal of Cleaner Production

journal homepage: www.elsevier.com/locate/jclepro

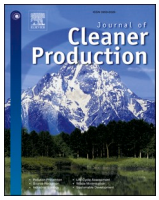

# A comprehensive comparative study of ultrasound-alkaline and thermal-alkaline hydrolysis of duck feather

Nidal Del Valle Raydan [a], Antoine Loquet [b], Birgit Habenstein [b], Brice Kauffmann [c], Bertrand Charrier [a], Gregory Chatel [d], Eduardo Robles [a,*]

[a] University of Pau and the Adour Region, E2S UPPA, CNRS, IPREM-UMR 5254, Mont de Marsan, France
[b] Univ. Bordeaux, CNRS, Bordeaux INP, CBMN, UMR 5248, IECB, F-33600, Pessac, France
[c] Univ. Bordeaux, CNRS, INSERM, IECB, US1, UAR 3033, F-33600, Pessac, France
[d] Univ. Savoie Mont Blanc, CNRS, EDYTEM, F-73000, Chambéry, France

ARTICLE INFO

Handling Editor: Xin Tong

*Keywords:*
Feather waste
Keratin
Ultrasound-assisted alkaline hydrolysis
Thermal alkaline hydrolysis
Efficiency
Sustainability

ABSTRACT

Feathers, as a byproduct of the poultry industry, present a significant source of keratinous waste. Conventional methods have been widely used to extract keratin from feathers; however, they are associated with limitations such as high operational costs and environmental concerns. It is, therefore, crucial to develop cost-effective and time-efficient methods for extracting keratin on a large scale. In recent years, ultrasound-assisted alkaline hydrolysis has emerged as a promising and sustainable approach for efficient keratin recovery. This study compares the hydrolysis time, yield, and chemical properties of keratin extracted from feathers using ultrasound-assisted alkaline hydrolysis and thermal alkaline hydrolysis (hot plate method). The influence of factors such as particle size, alkali concentration, liquid-to-solid ratio, reactor geometry, temperature of keratin colloid upon precipitation, precipitation pH, and precipitating acid was investigated. Favorable conditions for ultrasound-assisted alkaline hydrolysis were found to be 3% NaOH, a 10:100 (w/v) solid-to-liquid ratio, using a cylindrical vessel, and an ultrasonic energy density of 360 kJ/L, with pH adjustment to 4.5 using citric acid after cooling to room temperature. This method outperformed the thermal approach, yielding 70% keratin in 25 min, compared to 23% in 90 min using a hot plate, due to the exothermic effect of cavitation. The results provide valuable insights into the potential of ultrasound-assisted alkaline hydrolysis as an eco-friendly and cost-effective approach to address the management of keratinous waste and enhance the overall recovery of keratin.

## 1. Introduction

The European Union is a major player in the global poultry meat industry, boasting a substantial production capacity of approximately 13.4 million tons annually (European Commission, n.d.). In particular, France emerged as the leading producer of poultry meat by 2021, with a remarkable production volume of 1503.58 thousand tons in December of 2022, as reported by EUROSTAT (Eurostat, 2023). According to the latest expert forecast released on June 22, 2023, France's duck meat production has reached an outstanding volume of 140 thousand tons, further solidifying its position as the EU's leader in duck production (Expert Group for Agricultural Markets, 2023). With the growing consumption of poultry, there is a steady increase in the number of feathers generated as a byproduct. In Europe alone, the poultry sector generates approximately 3.6 million tons of feathers annually, which is considered a waste or a low-value byproduct (Farrelly & Mitchell, 2023). Enormous quantities of keratinous biomass are currently being disposed of through methods such as dumping, landfilling, and incineration, leading to significant environmental pollution on a global scale.

Consequently, it is necessary to explore effective approaches to treating this biomass. Feathers, primarily composed of keratin, offer one of the most abundant sources of keratinous biomass, with their keratin content ranging from 85% to 90% (Grazziotin et al., 2006). Keratin, a fibrous protein, possesses exceptional mechanical stability attributed to several factors, including abundant hydrophobic interactions, hydrogen bonds, and intramolecular/intermolecular disulfide cross-linking (Bragulla and Homberger, 2009). Two types of keratins can be found in nature: α-keratin and β-keratin, which can be distinguished based on their X-ray diffraction patterns. The α-keratin is found in several mammalian structures, including wool, hair, horn, nails, hooves, and the

* Corresponding author.
*E-mail address:* eduardo.robles@univ-pau.fr (E. Robles).

https://doi.org/10.1016/j.jclepro.2024.142927
Received 26 March 2024; Received in revised form 7 June 2024; Accepted 16 June 2024
Available online 21 June 2024

outermost layer of the skin called the stratum corneum. On the other hand, β-keratin is primarily present in the durable tissues of avian and reptilian species, including feathers, beaks, and talons of birds, as well as scales and claws of reptiles (Chen et al., 2012). The elasticity of keratin fibers results from the intricate interplay between the protein's helical and sheet-like structures. The presence of disulfide bonds formed between cysteine molecules plays a crucial role in enhancing the stability and reducing the solubility of keratin. These bonds occur within the protein chain and between different proteins, forming a robust three-dimensional structure (Callegaro et al., 2019). Consequently, the dissolution of feathers and extraction of keratin pose notable challenges, making it essential to identify an efficient, environmentally friendly, and cost-effective method. In recent years, significant progress has been made in the extraction and characterization of keratin, resulting in increased production of keratin-based materials. These materials have found extensive applications in industries such as cosmetics (Burnett et al., 2021; Mokrejs et al., 2017), pharmaceuticals (Sarma, 2022), leather (Pan et al., 2023), animal feed (Coward-Kelly et al., 2006), and agriculture (Chen et al., 2022). The commonly used methods for extraction from keratin-rich materials are chemical hydrolysis (Shavandi et al., 2017), thermal hydrolysis or superheated process (Bhavsar et al., 2017; Tasaki, 2020), dissolution in ionic liquids (Ji et al., 2014), microwave irradiation (Zoccola et al., 2012), enzymatic and microbial treatment (Kshetri et al., 2022; Qiu et al., 2020), and steam explosion (Zhang et al., 2015). However, traditional chemical extraction methods for keratin often rely on highly concentrated toxic agents. Using these products results in high operational costs and poses significant health and environmental risks. Additionally, these chemical processes can be time-consuming. For instance, hydrothermal processes commonly used to treat feather waste involve cooking feathers at high temperatures and pressures by adding acids or alkalis. This process aims to destroy the structure of hard-to-denature keratin in feathers and improve the solubility of feather components (Chilakamarry et al., 2021). However, longer time at high temperatures or pressure during hydrothermal treatment can cause excessive denaturation of certain amino acid sequences, causing loss of thermolabile amino acids (Hong et al., 2022).

Considering the drawbacks of hydrothermal methods mentioned above, ultrasound-assisted hydrolysis technology has been developed as an alternative approach for the recovery of keratin from feathers (Feroz et al., 2022; Holkar et al., 2016; Hong et al., 2022; Pedrosa et al., 2022). This method harnesses the phenomenon of cavitation, where the formation and rapid collapse of bubbles generate high temperature and pressure conditions (Mondal et al., 2021). Cavitation induces chemical and physical effects, including the possible decomposition of water molecules and the creation of free radicals (Riesz et al., 1985). Acoustic cavitation-assisted hydrolysis offers a cost-effective, environmentally friendly, and energy-efficient solution compared to other extraction processes (Hoo et al., 2022). However, despite the research conducted in this area, none of the alternative processes described in the literature have been successfully commercialized. This lack of commercialization can be attributed to the limited availability of comprehensive comparisons between alternative and conventional processes, the absence of extensive experiments exploring factors such as solvent concentration and precipitating acids, and challenges related to reproducibility and scalability. Moreover, a significant hurdle to commercialization is finding applications with substantial added value; thus, transforming waste into valuable products represents a challenging yet promising avenue for ultrasound technology.

The main aim of this work was to study the ultrasound-assisted alkaline hydrolysis (UAH) of duck feathers and compare it with thermal alkaline hydrolysis (TAH) at a temperature of 75 °C using NaOH as an alkali agent and different organic acids for the precipitation of keratin. This study explores the influence of various hydrolysis conditions on the extraction efficiency and quality of keratin extracted from duck feathers. The study's broader objective was to find an effective, eco-friendly method for high-yield, high-quality keratin recovery from poultry waste, enhancing its value through advanced hydrolysis techniques for industrial applications.

## 2. Materials and methods

### 2.1. Materials

The raw feather (RF) material utilized was white feathers from Mullard duck, generously supplied by an industrial partner (Plum'Export, Saint-Sever, France). The sample corresponds to the fraction of feathers discarded after selecting down and bristles, which the company sells for quilts and down jackets. Random feathers were analyzed in a prior study, having a moisture content of 9.15%, a protein content of 82.97%, a fat content of 0.98%, and an ash content of 0.68%, totaling 93.78% (Alvarez et al., 2023). The unaccounted 6.22% could include non-protein nitrogen and other trace components, which are not precisely quantified due to limitations in the analytical methods. Sodium hydroxide (NaOH, CAS number 1310-73-2), acetic acid (A.A., $CH_3COOH$ 64-19-7), oxalic acid (O.A., $(COOH)_2$, 144-62-7), citric acid (C.A., $HOC(CO_2H)(CH_2CO_2H)_2$, 77-92-9) sulfuric acid (S.A., $H_2SO_4$, 7664-93-9), and hydrochloric acid (H.A., HCl, 7647-01-0) used in this research work were purchased from Sigma-Aldrich.

### 2.2. Keratin unfolding and refolding

#### 2.2.1. Optimizing keratin unfolding parameters

Each parameter was optimized individually in this preliminary research phase, with only the most effective condition being carried forward to subsequent experiments. This sequential optimization approach was chosen due to the study's exploratory nature, focusing initially on understanding the individual effects of each variable on the process without examining their interactions. The complexity and number of variables precluded a complete interaction study.

The UAH experiments were conducted using a 500 mL round-bottom flask or a 500 mL beaker without further temperature control. Ultrasonic waves were introduced into the system using a 200 W ultrasonic processor (UP200St 26 kHz, Hielsher, Germany) with a 14 mm sonotrode (S26d14) set at an amplitude (A = 80%) of the maximum electric power of the device. The average efficiency of the machine is $5.10^{-3}$ Wh, which is calculated by directly measuring the difference between consumed energy using a wattmeter and comparing the results with the machine-generated value.

*2.2.1.1. Feeding size.* The RF underwent grinding using two distinct methods. The first was grinding the RF to 0.08 mm using (UC mill, ZM 200, Retsch). The second was grinding the RF to 1.5 mm using (RB, Electric Grain Mill Grinder, VEVOR) (Fig. S1). The choice of the specific powder size for the subsequent hydrolysis studies was supported by the investigation of the effects of grinding on the chemical and physical properties of RF.

*2.2.1.2. NaOH concentration.* The impact of NaOH concentration on feather hydrolysis and keratin properties was examined using three different NaOH concentrations: 1%, 3%, and 5% (V = 450 mL). The hydrolysis process maintained a L/S ratio, referring to the volume of alkaline solution (solvent) to the proportion of RF (material), of 100:2 (v/w). The keratin colloid was left to cool and precipitated with a pH of 4.5 with C.A. The collected dataset measured included Pre-US-pH and Post-US-pH, T in °C, t in min, E in kWh, and the quantity of acid used. Lyophilized keratins presented a differentiated surface layer of WKH, which was challenging to quantify due to its light weight (max 10% yield). In data tables, its presence is categorized as highly present (++), moderately present (+), or absent (−), systematically noting variations in keratin integrity post-treatment. The analyses that were conducted for the KH included ATR-IR, TGA, and DSC. The RY was obtained by

weighing $M_{dry}$. AY denoted by equation 1, was computed by contrasting the RY amount with $M_0$, determined through Kjeldahl's method (82.97 ± 0.98%).

Eq: 1: AY (%) = $[M_{dry}/ 0.83M_0]*100$

*2.2.1.3. L/S ratio.* The L/S ratio is critical in controlling ultrasound-assisted hydrolysis efficiency (Dzah and Dzigbor, 2023). Therefore, the influence of the L/S ratio on hydrolysis time and keratin properties was examined using five different ratios: 100:2, 100:4, 100:6, 100:8, and 100:10 (v/w). The hydrolysis process maintained a constant NaOH concentration of 3% based on previously selected outcomes. The keratin colloid was left to cool and precipitated with a pH of 4.5 with C.A. The dataset collected in the study included pre-US-pH and post-US-pH, T in °C, t in min, E in kWh, the quantity of acid used, yields (RY and AY), and WKH presence. The analyses that were conducted for the KH included ATR-IR, TGA, and DSC.

*2.2.1.4. Reactor geometry.* The consideration of reactor geometry is important when considering heterogeneous systems such as biomass hydrolysis, as the biomass may act as a reflector of the ultrasonic wave and effectively change the sonication region and directly the sonochemical efficiency and yield even if the remaining conditions are the same (Bussemaker, 2013). The study transitioned from using a round-bottom flask to a cylindrical vessel as a reactor to explore this effect. Based on previously selected outcomes, the hydrolysis process maintained a constant NaOH concentration of 3% and an L/S ratio of 100:10. The keratin colloid was left to cool and was precipitated with a pH of 4.5 with C.A. The dataset collected in the study included pre-US-pH and post-US-pH, T in °C, t in min, E in kWh, the quantity of acid used, and yields (RY and AY).

*2.2.2. Optimizing the refolding conditions*

*2.2.2.1. Temperature.* After the UAH, a determined acid was added to the keratin colloid after cooling to room temperature for precipitation at pH 4.5. The precipitated keratin was centrifuged at an RCF of 8765 g for 10 min, dialyzed against distilled water until a neutral pH (6–7) was obtained, and was then dried through lyophilization over at least 48 h until final drying was achieved by using a lyophilizer (Alpha 1–4, Martin Christ GmbH, Osterode am Harz, Germany) with a sublimation temperature of −80 °C.

The effect of the temperature of the keratin colloid before precipitation on keratin aggregation after precipitation was investigated. A keratin colloid of 100: 10 (v/w) obtained of 3% NaOH UAH was subjected to precipitation using C.A to reach a pH of 4.5 at three distinct temperatures: 25 °C, 50 °C, and 75 °C. It's important to note that after UAH, the keratin colloid is hot due to the exothermic reaction of cavitation, and thus it's essential to assess whether precipitation directly or after cooling is necessary. The aggregation process was observed at each temperature, the AY of KH was calculated, and its appearance was evaluated after precipitation and lyophilization. This approach evaluates how temperature before acid precipitation influences keratin recovery and aggregation. The resulting data provides insights into the optimal temperature for effective keratin refolding.

*2.2.2.2. pH.* The study examined the influence of pH on keratin precipitation. The keratin colloid obtained by 3% NaOH, UAH, was precipitated with C.A to two distinct pH levels: 4.5 and 3.5. At each of these pH values, the precipitation process was carefully monitored. Following this, the AY of KH was calculated, and its appearance was evaluated after precipitation and lyophilization. This approach aimed to understand how pH influences the efficiency of keratin precipitation and the physical properties of the KH.

*2.2.2.3. Acid used.* The study examined the effect of different acids used for keratin precipitation. To this, the keratin colloid of 100: 10 (v/w) obtained by 3% NaOH UAH was precipitated with the organic acids (A. A, O.A, and C.A) for comparison with S.A and H.A. Throughout the hydrolysis process, the collected dataset measured included Pre-US-pH and Post-US-Ph, T in °C, t in min, E in kWh, quantity of acid used, yields (RY and AY), and WKH presence. The analyses that were conducted for the KH included FTIR, TGA, and DSC.

*2.2.3. Thermal alkaline hydrolysis (TAH): comparative study of optimized conditions*

The hydrolysis process was conducted at 75 °C using a hot plate stirrer. This specific temperature was selected to facilitate a more effective comparison with ultrasound-assisted hydrolysis, which naturally reached this temperature as average due to the absence of temperature control. The RF was continuously stirred at 800 rpm and heated until complete hydrolysis was achieved. Like previous trials, hydrolysis maintained a 100:10 (v/w) and a 3% NaOH concentration. Furthermore, the keratin colloid was precipitated with the organic acids (A.A, O.A, and C.A) and two inorganic acids for comparison (S.A and H.A). The recorded dataset included pre- and post-US pH, T in °C, t in min, E in kWh, the quantity of acid used, yields (RY and AY), and WKH presence. The analyses that were conducted for the KH included FTIR, TGA, and DSC.

## 3. Characterization methods

### 3.1. Chemical and structural characterization

SDS-PAGE analysis was performed using Laemmli's method (Laemmli, 1970) for RF (Restch and Vevor), and the selected KH obtained from both UAH and TAH. A bovine albumin standard (2 mg/mL) was used as a reference. All samples were incubated for 5 min at 95 °C in 2x buffer of 250 mM Tris-HCl (pH 6.8), 8% SDS, 40% glycerol, 8% 2-mercaptoethanol, and 0.02% bromophenol blue. For the gel, 10 μL of Prestained Protein Ladder (10–250 kDa) was loaded in lane 1, while 10 μL of the different samples and bovine albumin were loaded in separate wells of the subsequent lanes. The electrophoresis process utilized Bolt™ 4–12% Bis-Tris Plus Gel (Invitrogen™ NW04120BOX, USA) and SDS running buffer. The gels were run at 180 V until the dye front reached the bottom of the gel. Following electrophoresis, the gels were stained with Coomassie Brilliant blue R 250 and rinsed with 5% acetic acid and 20% methanol until a clear background was observed.

Functional groups of the feathers and the KHs were analyzed using Attenuated Total Reflectance (ATR) mode in an ATR-IR spectrometer (FT/IR-4700, Jasco). All spectra were recorded over a 4000-400 $cm^{-1}$ range using 64 scans and 2 $cm^{-1}$ resolution. These spectra were normalized to the amide I band at 1632 $cm^{-1}$.

Solid-state NMR experiments were recorded at room temperature on a 5500 MHz spectrometer (Bruker BioSpin) using a 4 mm double resonance probe under magic-angle spinning conditions (11 kHz). $^{13}C$-detected spectra were obtained using an initial cross-polarization with a contact time of 1 ms or an INEPT polarization transfer. High-power decoupling (SPINAL-64) (Fung et al., 2000) was applied during acquisition. Chemical shifts were calibrated and referenced with DSS.

X-ray diffraction experiments were performed on a Rigaku FRX rotating anode at the copper kα wavelength using a Hybrid Pixel detector (HyPix6000 from Rigaku). MicroMeshes from MiTeGen® were used as powder sample holders on the goniometer head. Each diffraction pattern represents a 360° rotation along the ϕ axis, with an exposure time of 720 s. No corrections, such as a smooth filter or baseline correction, were applied to the data. WinPLOTR (https://cdifx.univ-rennes1.fr/winplotr/winplotr.htm) was used to generate the 2D plots.

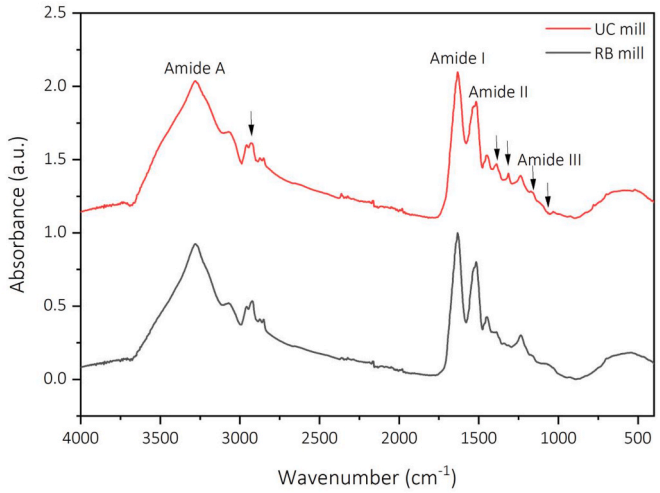


**Fig. 1.** ATR-IR spectra of RF processed using a) UC mill and b) RB mill.

### 3.2. Morphology

Scanning electron microscopy (SEM) was used to study keratin hydrolysates. Samples were mounted onto specific stubs and coated with platinum using a sputter coater (Q150T, Quorum Technologies, Kent, UK). Observations were done at 2 kV, in high vacuum mode, with an electronic microscope (Gemini SEM 300 FESEM, Zeiss, Germany).

### 3.3. Thermal analysis

The thermal resistance of the different ground feathers and KH were measured and conducted in a TA Q500 thermogravimetric analysis; samples were heated from 30 °C to 800 °C at a rate of 10 °C/min under a nitrogen atmosphere. The melting temperatures of different ground feathers and KH were measured using a TA Q20 differential scanning calorimetry under a continuous nitrogen purge at a heating rate of 10 °C/min over a temperature range of −50 °C–250 °C.

## 4. Results and discussion

### 4.1. Keratin unfolding and refolding

#### 4.1.1. Keratin unfolding: UAH optimization parameters

##### 4.1.1.1. Feeding size

*4.1.1.1.1. ATR-IR spectroscopy.* ATR-IR analysis was carried out for ground RF processed using UC and RB mills to identify the functional groups altered or lost due to high friction and temperature experienced during grinding. The resulting FTIR spectra in Fig. 1 show clear distinctions, suggesting alterations in the main functional groups due to the grinding stress. The approximate peak assignments and corresponding wavenumbers are shown in Table S1. Spectral differences around 1076 $cm^{-1}$ and 1238 $cm^{-1}$ indicate a decrease in cystine monoxide (R–SO–S-R) and cystine dioxide (R–$SO_2$-S-R) structures in the UC mill, which probably aligns with the observed emission of smoke during the burn, which is referenced in prior studies as possibly $SO_2$ (Turner and Sapp, 2023). Additionally, the band at 1312 $cm^{-1}$ is ascribed to either O–H deformation or $CH_2$ wagging motions, and the band at 1388 $cm^{-1}$ C–H bending vibration, which became more prominent in the UC mill, indicating changes in the methylene groups' environment and the keratin structure due to heat. The concurrent reduction in methyl C–H asymmetric and symmetric stretching bands, at 2922 $cm^{-1}$, further supports the hypothesis of thermal decomposition of methyl groups within the amino acids of the feather keratin. The fact that the amide bands are still detectable but reduced after heat exposure implies that while some peptide bonds were disrupted, the keratin's overall structure exhibited thermal stability.

*4.1.1.1.2. TGA and DSC analysis of RF processed through UC and RB mills.* The Thermogravimetric Analysis (TGA) presented different thermal degradation profiles for the RF samples processed by UC and RB mills (Fig. 2a). The initial weight loss below 150 °C corresponds to moisture loss and bound water. The UC sample was more dehydrated than the RB sample due to the burning, which showed less weight loss in the initial phase than the RB sample. As the temperature increased, the UC sample began to degrade at a higher temperature, around 290 °C, indicative of a delayed onset compared to the RB sample, which started around 235 °C. This delay for the UC sample might imply a more stable alpha-helix structure formed after the dehydration of the protein, promoting tighter packing of the alpha-helices, as water is often associated with the disruption of hydrophobic interactions that stabilize the helical structure (Shi et al., 2001). However, once degradation started, the UC sample exhibited a more rapid decline, with a sharper and more pronounced weight loss, particularly beyond 350 °C, resulting in 76% loss compared to 68% for the RB sample at 500 °C. This rapid degradation indicates reduced thermal stability of the UC sample due to structural and chemical changes induced by the frictional heat during grinding, which could result from a higher degree of disorder in the secondary structure, breaking down some of the protein's tertiary structures and weakening the overall material.

The DSC analysis (Fig. 2b) showed differences between the RF processed using UC and RB mills. The UC sample showed a broadened

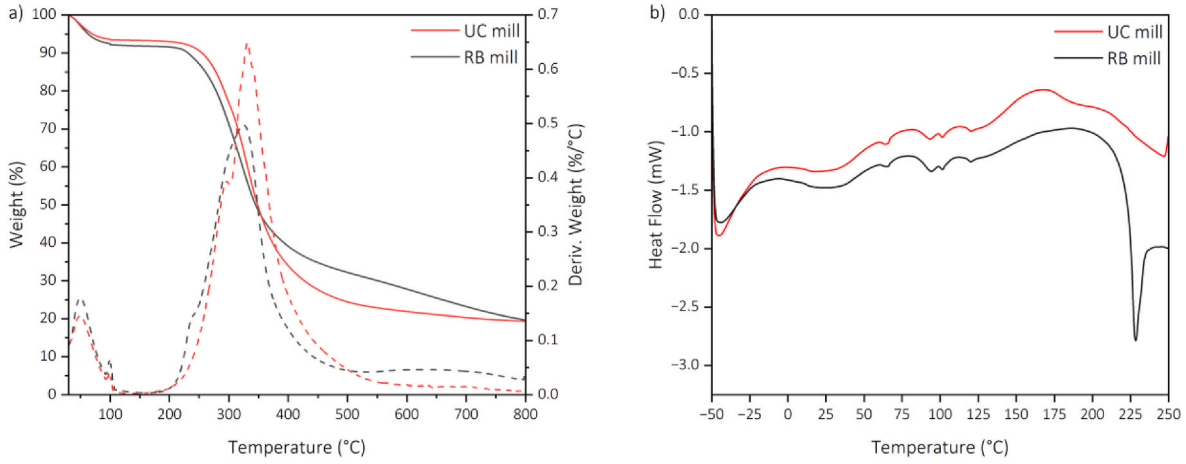


**Fig. 2.** Thermogravimetric Analysis (TGA) and Differential Scanning Calorimetry (DSC) of RF processed using UC and RB mills.

**Table 1**
Abbreviations used in the study.

| Abbreviation | Full Name |
|---|---|
| UAH | Ultrasound-Assisted Alkaline Hydrolysis |
| TAH | Thermal Alkaline Hydrolysis (Hot plate) |
| RF | Raw feather |
| NaOH | Sodium Hydroxide |
| A.A. | Acetic Acid |
| O.A. | Oxalic Acid |
| C.A. | Citric Acid |
| S.A. | Sulfuric Acid |
| H.A. | Hydrochloric Acid |
| UC | Ultra-Centrifugal |
| RB | Rotational Blade |
| L/S ratio | Liquid-to-Solid Ratio |
| V | NaOH Volume |
| Pre-US-pH | pH before hydrolysis |
| A | Amplitude |
| Post-US-pH | pH after hydrolysis |
| T | Post-hydrolysis temperature |
| t | Hydrolysis time |
| E | Energy consumption |
| KH | Keratin hydrolysate |
| ATR-IR | Attenuated Total Reflection Infrared Spectroscopy |
| TGA | Thermogravimetric Analysis |
| DSC | Differential Scanning Calorimetry |
| RY | Relative Yield |
| AY | Absolute Yield |
| $M_{dry}$ | Weight of keratin hydrolysate after lyophilization |
| $M_0$ | Initial keratin content in the RF |
| WKH | Cotton-like White Keratin Hydrolysate |
| ++ | Highly present |
| + | Moderately present |
| – | Absent |
| RCF | Relative Centrifugal Force |
| SDS-PAGE | Sodium Dodecyl Sulfate Polyacrylamide Gel Electrophoresis |
| SEM | Scanning Electron Microscopy |
| NMR | Nuclear Magnetic Resonance |
| XRD | X-Ray Diffraction |

endothermic peak within the 225–250 °C range, suggesting a wide range of structural alterations. These alterations contrast the sharper transition observed in the RB attributed to crystalline α-helix disordering or melting (Yimer, 2017). The UC sample's endothermic peak, typically linked to α-helix decomposition, was almost absent, likely due to the structural disorder introduced by grinding. This decomposition aligns with the TGA results of the UC, which indicated a delayed but fast decomposition, and with FTIR findings of an altered structure obtained in the UC sample. These analyses suggest that RFs processed under stress (UC) have a more disrupted structure and less thermal stability than those processed more gently (RB). Therefore, for subsequent hydrolysis studies, RF was ground to a size of 1.5 mm using RB, ensuring a consistent and reliable starting material.

*4.1.1.2. Effect of NaOH concentration on UAH and KH yield.* Alkali hydrolysis facilitates the cleavage of cystine disulfide bonds in feather keratin, typically enhanced by applying heat and increased alkali concentration (Staroń et al., 2014). The data in Table 2 indicate that higher NaOH concentrations reduce the time necessary for complete hydrolysis. Additionally, more rapid hydrolysis processes are associated with lower final temperatures, likely due to the thermogenic effect of ultrasound cavitation. The study found that lower NaOH concentrations (1% NaOH) and temperatures (64 °C) were more effective in preserving keratin yield. Despite the final temperature for 5% NaOH being comparable to that of 1% NaOH, the higher concentration of NaOH appears to contribute to a more significant keratin degradation, as reflected by the lower yields (AY = 2.68%). Moreover, the keratin precipitated rapidly and evenly in the case of 1% NaOH, whereas keratin from the 5% NaOH solution showed slower and bulkier precipitation, resulting in a darker color upon drying. This degradation may confirm that higher alkaline conditions during UAH may lead to more extensive breakdown of keratin into smaller peptide fragments.

Moreover, lyophilized samples displayed WKH on the surface (Fig. S2). This phenomenon can likely occur during congelation, as this process is not instantaneous; unlike freezing in nitrogen liquid, it generally starts from the edges towards the center or the top down, preferentially incorporating pure water and excluding solutes, which are

**Table 2**
Effect of NaOH concentration on UAH hydrolysis and KH yield, showing variations in process parameters and results. Abbreviations are defined in Table 1.

| NaOH (%) | V (mL) | RF (g) | Pre-US pH | A (%) | E (kWh) | t (min) | Post-US pH | Temp (°C) | C.A (g) | RY (g) | AY (%) | WKH |
|---|---|---|---|---|---|---|---|---|---|---|---|---|
| 1 | 450 | 9 | 13.20 | 80 | 0.057 | 35 | 12.51 | 64 | 14 | 1.73 ± 0.35 | 23.16 ± 4.66 | ++ |
| 3 | 450 | 9 | 13.57 | 80 | 0.045 | 25 | 13.02 | 80 | 37 | 1.04 ± 0.11 | 13.85 ± 1.44 | ++ |
| 5 | 450 | 9 | 13.67 | 80 | 0.029 | 15 | 13.24 | 65 | 58 | 0.20 ± 0.08 | 2.68 ± 1.10 | ++ |

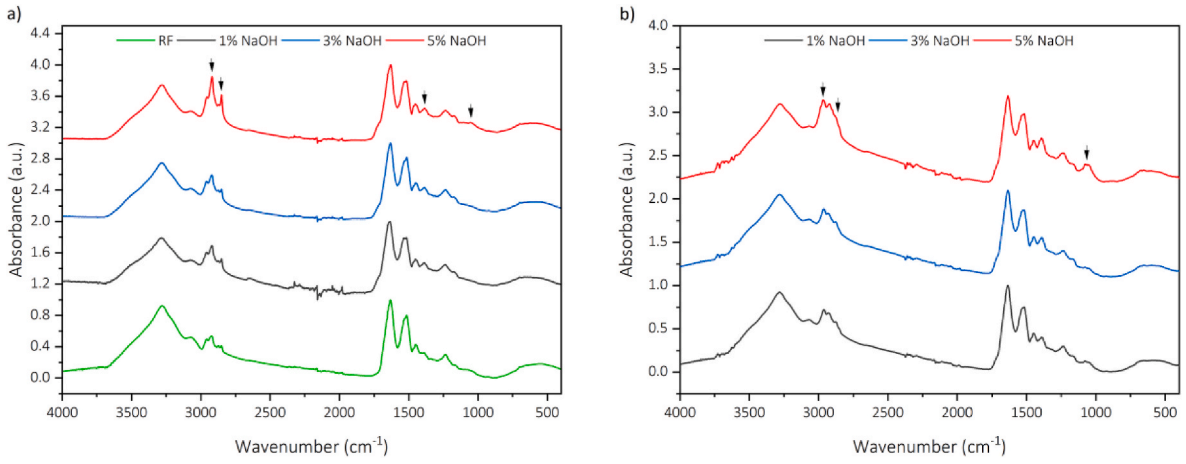


**Fig. 3.** ATR-IR spectra of a) KH obtained from different NaOH concentrations compared to RF, and b) WKH obtained from the surface of the same samples at different NaOH concentrations.

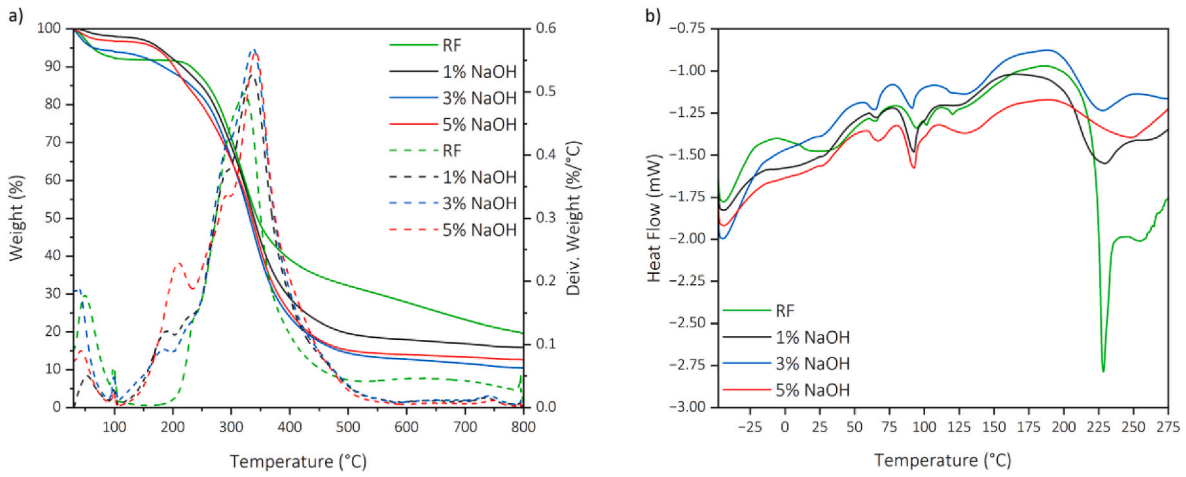


**Fig. 4.** TGA (a) and DSC (b) of KH obtained from different NaOH concentrations compared to RF.

the higher-weight keratin. This sedimentation can cause the lower-weight suspended keratin to freeze earlier with pure water on the surface. Lower NaOH concentrations and reduced temperatures were more advantageous to higher yields, suggesting that these milder conditions are less disruptive to the amino acid integrity of the keratin.

*4.1.1.2.1. ATR-IR spectroscopy.* ATR-IR analysis was carried out for the KH from UAH with different NaOH concentrations (1%, 3%, and 5%) to identify the functional groups altered due to high alkaline concentration and temperature experienced during hydrolysis. The resulting FTIR spectra in Fig. 3a show clear distinctions in the keratin obtained for the 5% hydrolysis but not the 1% NaOH and the 3% NaOH, suggesting alterations in the main functional groups due to the high alkalinity that are not present in RFs, according to the approximate band assignments and corresponding wavenumbers in Table S1.

Spectral differences around 1176-1032 $cm^{-1}$ for the cystine band indicate an alteration in the cystine structure in the 5% NaOH keratin. According to previous studies, cystine can be transformed into lanthionine under strongly alkaline conditions, called lanthionization reaction, which causes the cleavage of the cystine disulfide bond ($–CH_2–S–S–CH_2–$) and its replacement with a lanthionine bond ($–CH_2–S–CH_2–$), a stable thioether bond (Boga et al., 2014; Papadopoulos, 1985). The increase in the symmetric and asymmetric stretching of C–H bonds in methylene groups ($–CH_2–$), at 2877 and 2922 $cm^{-1}$, respectively, suggest further the alteration of keratin structure and its transformation to other amino acids of alkyl side chains. These were lower in the WKH of the same sample (Fig. 3b). Moreover, there was an increase in the 2966 $cm^{-1}$ band in the WKH corresponding to the asymmetric stretching of C–H bonds in methyl groups ($–CH_3–$), which can be due to the presence of more terminal amino acids or side chains that contain methyl groups that result from the smaller peptide. A band between 1050 and 1075 $cm^{-1}$, unique to WKH, indicates S–O stretching vibrations, which can imply the presence of sulfate groups or cystine monoxide. Sulfates in keratin could arise from incorporating sulfur from cysteic acid formed from cysteine oxidation. No noticeable differences in the profile of the amide I and II bands were observed as a function of the NaOH concentration.

*4.1.1.2.2. TGA and DSC analysis of KH from UAH with different NaOH concentrations.* The Thermogravimetric Analysis of KH from UAH with varying NaOH concentrations revealed distinct thermal degradation behaviors (Fig. 4a). The initial weight loss near 100 °C for all samples is attributed to moisture evaporation. Further weight loss around 170–180 °C, particularly in the 1% and 3% NaOH samples, aligns with the release of bound water, potentially reflecting differences in bound water content or structural binding, whereas this weight loss is observed at 208 °C in the 5% NaOH sample. As the temperature increased beyond 200 °C, a notable weight loss occurred, particularly in the 1% and 3% NaOH samples around 225 °C, while the 5% NaOH sample demonstrated a later steeper decline, indicating higher alfa helix content in the 1% NaOH sample and less in the 3% NaOH sample, whereas an alteration of this structure in that of 5% NaOH sample. Around 285 °C, a plateau was observed for the 1% NaOH sample, indicating the degradation of beta-sheet structures, and a more pronounced plateau in the 3% NaOH sample may suggest a conversion from alpha-helices to beta-sheets at that alkali concentration during hydrolysis. Complete degradation of the samples occurred by approximately 500 °C, with a residual mass indicating carbon content, whereas the 1% NaOH sample showed a slightly higher residue, reflecting a potentially more extensive carbonization process.

Differential Scanning Calorimetry analysis of the KH further showed the structural transformations at various temperatures (Fig. 4b). Around 100 °C, endothermic peaks corresponding to moisture loss were observed for all NaOH concentrations. A notable peak at approximately 230 °C, particularly distinct in the 1% NaOH hydrolysate, was attributed to the melting of crystalline alpha-helix structures, implying a higher alpha-helix content and stability at lower alkali concentrations. The 5% NaOH sample exhibited this transition at a higher temperature of around 250 °C, with a less defined peak, suggesting a reduction or destabilization of alpha-helix content. This melting point shift suggests that increased NaOH concentration may disrupt alpha-helical structures. Meanwhile, the 3% NaOH sample showed an intermediate behavior, with its alpha-helix melting peak being less defined than that of the 1% sample, indicating that a moderate alkali concentration might facilitate

**Table 3**
The effect of the L/S ratio on UAH hydrolysis and KH yield shows variations in process parameters and results. Abbreviations are defined in Table 1.

| L/S Ratio | RF (g) | $V_{Total}$ (mL) | NaOH (%) | Pre-US pH | A (%) | E (kWh) | t (min) | Post-US pH | T (°C) | C.A (g) | RY (g) | AY (%) | WKH |
|---|---|---|---|---|---|---|---|---|---|---|---|---|---|
| 2:100 | 9 | 450 | 3 | 13.67 | 80 | 0.045 | 25 | 13.24 | 81 | 37 | 1.04 ± 0.11 | 13.85 ± 1.44 | ++ |
| 4:100 | 18 | 450 | 3 | 13.67 | 80 | 0.048 | 25 | 12.98 | 81 | 37 | 2.12 ± 0.22 | 14.15 ± 1.44 | ++ |
| 6:100 | 27 | 450 | 3 | 13.59 | 80 | 0.044 | 25 | 12.97 | 80 | 37 | 3.92 ± 1.27 | 17.47 ± 3.41 | + |
| 8:100 | 36 | 450 | 3 | 13.59 | 80 | 0.044 | 25 | 12.87 | 78 | 37 | 6.64 ± 1.28 | 22.24 ± 4.29 | ++ |
| 10:100 | 45 | 450 | 3 | 13.56 | 80 | 0.043 | 25 | 12.88 | 75 | 37 | 18.73 ± 1.64 | 50.15 ± 4.38 | – |

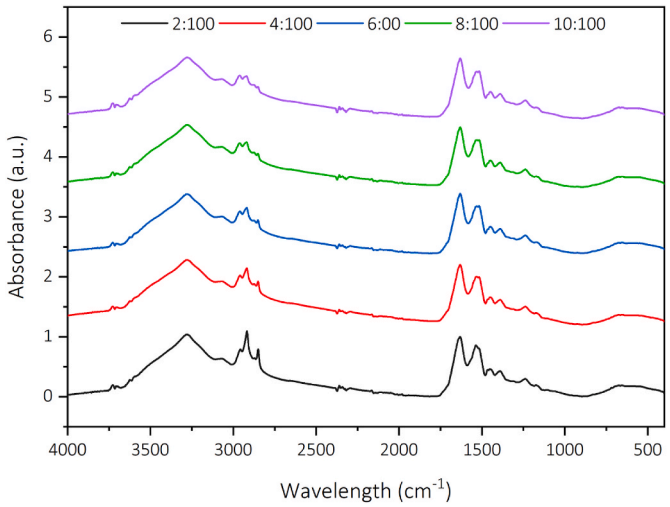


**Fig. 5.** ATR-IR spectra of KH obtained from UAH of different L/S.

the transformation of alpha-helices to beta-sheets, as deduced from the TGA results.

While (1% NaOH) yielded the highest keratin recovery, the faster process was prioritized for further optimization, leading to the selection of (3% NaOH). Specifically, using 3% NaOH significantly reduced the hydrolysis time, an important factor when considering the limitations of ultrasound treatments. Prolonged exposure to NaOH during these treatments can corrode the sonotrode probe, and thus, shorter hydrolysis times are preferable to preserve the equipment. This decision aligns with optimizing the hydrolysis process for scalability and practical application, where time efficiency and equipment preservation are paramount.

*4.1.1.3. Optimizing the L/S ratio for subsequent extractions.* Table 3 shows a positive correlation between the L/S ratio and keratin yield, with a decrease in the final hydrolysis temperature. Despite varying the ratios, the time needed for hydrolysis to complete without temperature control was the same, confirming that hydrolysis time is influenced by the NaOH concentration rather than the density of the medium. The L/S ratio has emerged as a critical factor, directly influencing ultrasound power intensity within the medium as shown in previous studies, in which adequate transfer of acoustic energy into the medium is essential for effective cell disruption and solute mass transfer *via* acoustic cavitation, which can significantly enhance the extraction of desired compounds. Conversely, there is negligible acoustic cavitation and high ultrasound power attenuation in dense and viscous media due to ultrasound waves' decreased propagation speed (Dzah and Dzigbor, 2023; Chen et al., 2013). The observed lower temperatures at higher L/S ratios suggest an attenuation of ultrasound power. A more diluted system with a lower L/S ratio allows for more extensive keratin degradation due to increased heat generation and effective cavitation.

Furthermore, white, cotton-like keratin on the surface is more pronounced at higher temperatures and is notably absent at lower ones, such as 75 °C at 3% NaOH concentration. This phenomenon suggests that higher temperatures, which are more prevalent in diluted mixtures, may contribute to the shortening of keratin chains to smaller peptides during hydrolysis, thus leading to the formation of the observed lower molecular weight, WKH on the surface after lyophilization. The precipitated keratin at various L/S ratios during acidification is presented in Fig. S3. As the L/S ratio increased, a denser and more powdered form of keratin was observed, deviating from the bulkier appearance at lower ratios. Additionally, a whiter color keratin was observed with increasing solid content upon drying.

*4.1.1.3.1. ATR-IR.* In the ATR-IR spectra of the KH from UAH with varying L/S ratios (Fig. 5), the absorbance bands at 2920 $cm^{-1}$ and 2850 $cm^{-1}$ corresponding to the asymmetric and symmetric stretching vibrations of methylene ($CH_2$) groups decrease with an increase of L/S ratio. This behavior indicates less alteration of the cystine structure, which was previously explained, and maybe less lanthionization reaction. This observation aligns with the higher yields noted at increased L/S ratios, likely due to reduced cleavage of cystine disulfide bonds. The spectra did not show significant variations in the amide I and II bands across different L/S ratios, indicating that these protein secondary structures remain relatively unchanged under these conditions.

*4.1.1.3.2. TGA and DSC analysis of KH from UAH of different L/S.* The TGA curves for KH obtained through UAH at different L/S ratios reveal distinct thermal behaviors (Fig. 6a). Initially, a peak around 100 °C is consistent across all ratios, likely representing the evaporation of free water. The plateau observed around 150 °C for the 6:100 and 10:100 ratios, shifting to just before 200 °C for the 8:100 ratio, suggests the release of more tightly bound water molecules, possibly from within the keratin's structural matrix. The pronounced peak for the 2:100 and 4:100 ratios at 205 °C could indicate additional bound water release or the commencement of thermal degradation of lower volatile components. A sharp increase in weight loss rate peaking around 330 °C suggests the onset of rapid decomposition, likely due to the breakdown of the more stable keratin structures, such as the disulfide bonds of cystine, which was highest for the 10:100 and 8:100 likely due to the cystine preservation, unlike that of 2:100 and 4:100 with more cystine losses during hydrolysis. Complete decomposition at approximately 500 °C is observed, with the 8:100 and 10:100 ratios leaving behind a higher

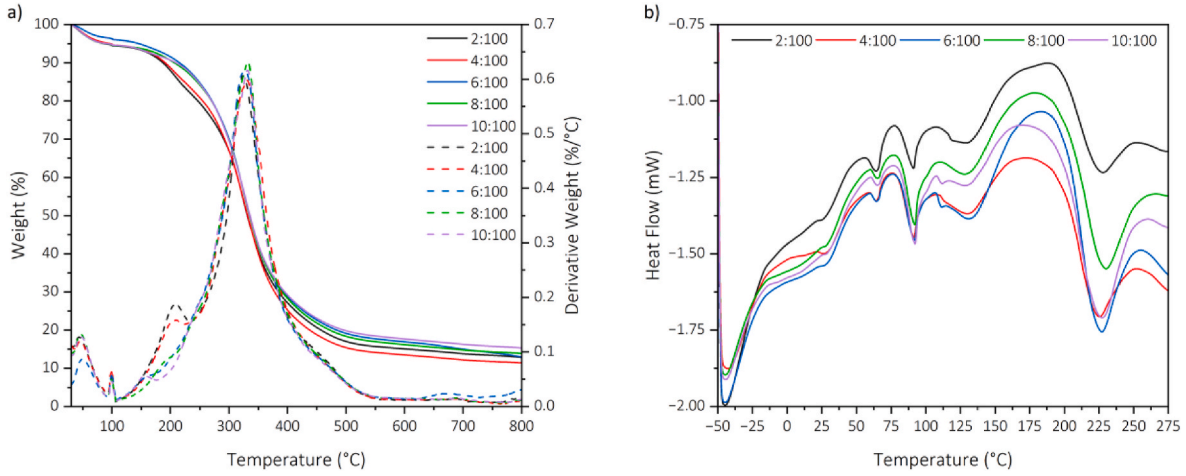


**Fig. 6.** TGA (a) and DSC (b) of KH from UAH of different L/S.

**Table 4**
Effect of reactor geometry on UAH hydrolysis and KH yield, showing variations in process parameters and results. Abbreviations are defined in Table 1.

| Flask geometry | RF (g) | $V_{Total}$ (mL) | NaOH (%) | Pre-US pH | A (%) | E (kWh) | t (min) | Post-US pH | T (°C) | C.A (g) | RY (g) | AY (%) | WKH |
|---|---|---|---|---|---|---|---|---|---|---|---|---|---|
| Round-bottom | 45 | 450 | 3 | 13.56 | 80 | 0.043 | 25 | 12.88 | 75 | 37 | 18.73 ± 1.64 | 50.15 ± 4.38 | – |
| Cylindrical | 45 | 450 | 3 | 13.56 | 80 | 0.043 | 25 | 12.85 | 65 | 37 | 26.22 ± 1.21 | 70.20 ± 3.24 | – |

carbon residue, indicating a larger proportion of non-volatile, carbon-rich material remaining after thermal degradation. In contrast, the lower ratios (2:100 and 4:100) end with the most minor residue, possibly due to a more complete breakdown or volatilization of their constituents.

The DSC analysis of KH across different L/S ratios (Fig. 6b) presents a complex thermal profile that varies with the composition of the samples. An endothermic peak around 90–100 °C, observed for the 10:100 and 6:100 ratios, indicates water loss or the transition of loosely bound water molecules, which occurs later for the 8:100 ratio and is latest for the 2:100 ratio. This delay in thermal response could reflect differences in the hydration levels or the binding affinity of water to the keratin matrix. All samples exhibit an endothermic event around 130 °C, which could correspond to further loss of bound water or other volatile components. The exothermic peak near 180 °C might be associated with the breakdown of organic components. This exothermic reaction leads to an important endothermic peak at approximately 230 °C, which signifies the melting of alpha-helix structures within the keratin. The most pronounced melting occurs in the 6:100 ratio, followed by 10:100 and 4:100, whereas the 8:100 and particularly the 2:100 ratios exhibit the smallest endothermic peaks, suggesting a potential reduction in alpha-helical content or alterations in protein stability.

Therefore, the 10:100 L/S ratio was selected for further hydrolysis studies based on its higher cystine preservation and enhanced thermal stability. This ratio also aligns with eco-friendly practices by reducing solvent use, thereby enhancing the sustainability of the process. Furthermore, the increased yield observed suggests that this ratio is more effective for keratin recovery, which is beneficial for scaling up production.

*4.1.1.4. Reaction flask geometry.* Table 4 reveals that switching from a round-bottom flask to a cylindrical vessel increased the absolute yield (AY) of keratin hydrolysis (KH) from 50% to 70% while reducing the final hydrolysis temperature from 75 °C to 65 °C. This temperature drop suggests an attenuation of ultrasound power in the cylindrical vessel again due to different wave propagation, impacting keratin yield (Fig. S4). The round-bottom flask's curved walls may focus ultrasound waves more effectively in the center than the flat walls of a cylindrical vessel, in which more dispersed wave patterns lead to less intense cavitation (Fig. S4). This finding underscores the importance of considering reactor geometry and temperature in optimizing hydrolysis processes, as supported by similar findings in other studies (Calinescu et al., 2019).

### 4.1.2. Optimizing the refolding conditions

*4.1.2.1. Temperature.* Proper refolding conditions must be found for every protein to ensure optimal yield. Unfolded proteins can easily aggregate during refolding through the various intermediate states (Yazdanparast et al., 2007). Many factors have been found to affect protein aggregation during refolding. These include temperature, protein concentration, type and concentration of denaturant, pH, ionic strength, refolding catalysts, thiol/disulfide agents, and miscellaneous additives (Wang et al., 2010).

In the study of keratin precipitation from a colloid solution, temperature was identified as a crucial factor affecting protein aggregation. As shown in Figs. S5a and S5b, varying the temperature of the keratin colloid prior to acid-induced precipitation resulted in different outcomes. At a higher temperature of 75 °C, there was a notable increase in protein aggregation, while at the lower temperature of 25 °C, keratin precipitated into a fine powder without aggregation. The temperatures studied were substantial in this case as they highlight the importance of not precipitating immediately after hydrolysis but rather after the colloid has cooled down. Notably, the absolute yield (70.78 ± 2.14 %) was not affected in this case; however, the physical aggregations were retained upon post-lyophilization. The increased protein aggregation at elevated temperatures can be ascribed to enhanced kinetic energy within the system. This energy augmentation leads to more vigorous molecular movement and a higher rate of collisions between protein molecules, which in turn raises the probability of hydrophobic interactions that can promote aggregation (Helmick et al., 2023; Jonas, 1997; Wang et al., 2010).

*4.1.2.2. pH.* Another type of aggregation may occur when the pH falls below the target value due to a higher acid quantity added. Precipitating keratin at a pH lower than its isoelectric point, at pH 3.5 instead of 4.5, can expose functional groups typically buried within the interior of the protein structure. These exposed regions can interact with similar patches on other protein molecules, forming a paste-like aggregate visible in Fig. S5c. This results in a softer, more malleable material that can be molded or reshaped. Subsequent lyophilization of this paste

**Table 5**
The effect of different precipitating acids on UAH hydrolysis and KH yield shows variations in process parameters and results. Abbreviations are defined in Table 1.

| NaOH (%) | R. F (g) | $V_{Total}$ (mL) | Pre-US pH | A (%) | E (kWh) | t (min) | Post-US pH | T (°C) | Acid used | Acid quantity (g) | RY (g) | AY (%) | WKH |
|---|---|---|---|---|---|---|---|---|---|---|---|---|---|
| 3 | 45 | 450 | 13.64 | 80 | 0.048 | 25 | 13.05 | 66 | Acetic | 32 | 23.91 ± 0.90 | 64.02 ± 2.42 | – |
| 3 | | | 13.57 | | 0.043 | 25 | 12.84 | 69 | Oxalic | 23 | 26.22 ± 1.63 | 70.20 ± 4.36 | + |
| 3 | | | 13.45 | | 0.045 | 25 | 12.89 | 65 | Citric | 25 | 26.73 ± 1.93 | 71.57 ± 5.18 | – |
| 3 | | | 13.44 | | 0.045 | 25 | 12.56 | 74 | Sulfuric (96%) | 20 | 22.54 ± 1.92 | 60.35 ± 5.13 | ++ |
| 3 | | | 13.49 | | 0.048 | 25 | 12.72 | 72 | Hydrochloric (37%) | 36 | 22.32 ± 0.45 | 59.76 ± 1.20 | ++ |

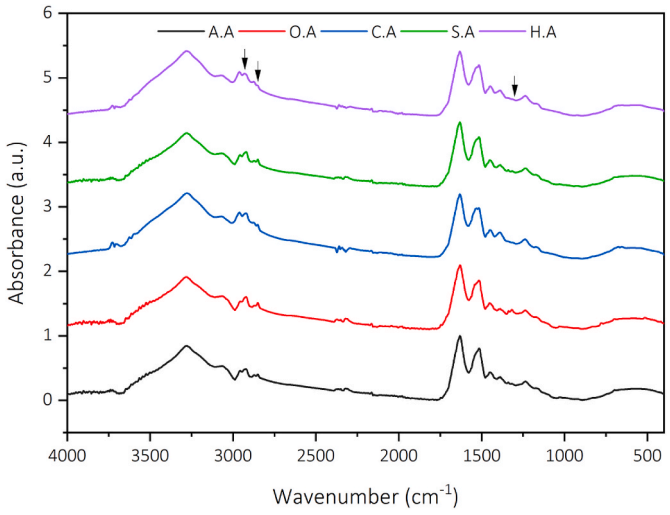


**Fig. 7.** ATR-IR spectra of KH obtained from UAH precipitated by different acids.

yielded a low absolute yield (AY = 9.62 ± 0.72 %), and the keratin obtained was only WKH. It possibly consists of smaller peptides cleaved from the main protein chain during hydrolysis or failed to refold properly due to the acidic conditions. These smaller peptides would have different solubility and isoelectric points.

*4.1.2.3. Acid used.* Different acids were applied to determine the most effective one for keratin recovery while considering the quantity of acid required to reach the target pH and the resulting yield in the study of investigating the impact of various acids on the precipitation of keratin UAH; the selected parameters were L/S of 100:10 and 3% NaOH concentration. Table 5 shows the quantity of acid needed to adjust the pH, revealing the relative strength of the acids used. Based on the data, sulfuric acid (96%), being the strongest, required the least volume (20 g), followed by hydrochloric acid (37%) (36 g). In contrast, organic acids needed more substantial amounts; oxalic acid required 23 g, citric acid 25 g, and acetic acid 32 g to achieve the same target pH of 4.5.

When comparing yields, citric acid led to the highest keratin recovery, followed by oxalic, acetic, sulfuric, and hydrochloric acids in descending order. This trend could be attributed to the aggressive nature of stronger acids, such as sulfuric and hydrochloric, which necessitate careful, dropwise addition and vigorous stirring to prevent keratin degradation by the acids. Organic acids like citric acid, milder and less reactive, do not pose the same risk of degrading keratin upon immediate contact and hence can lead to a more homogeneous and higher quality precipitate, as shown in Fig. S6.

Additionally, during the dialysis step, it was observed that oxalic acid caused the cellulose membranes to become matte and white, a phenomenon not seen with citric or other acids, as seen in Fig. S7. This effect might be explained by oxalic acid's unique chemical interactions with present metals, possibly leading to the formation of sodium oxalate ($Na_2C_2O_4$), which is insoluble and would lead to the observed whitening of the membranes. Unlike the more soluble sodium citrate or sodium acetate, sodium oxalate, formed during the neutralization of oxalic acid with sodium ions from the NaOH used in hydrolysis, has reduced solubility (Sigma Aldrich, 2024). This solubility could lead to its precipitation on the cellulose membranes used in dialysis or within the keratin matrix, manifesting as a white, matte appearance on the membranes or altering the texture of the keratin precipitate.

The presence of this oxalate was shown in the ATR-IR of the different membranes in Fig. S8, in the band 1316 $cm^{-1}$ and the strong band in the region 1612 $cm^{-1}$ corresponding to the symmetric and asymmetric stretching vibrations of the $COO^-$ group. Additional bands at 1315 $cm^{-1}$ ($\nu sym_{(COO-)}$), 796 $cm^{-1}$ ($\delta_{o\text{-}c=o} + \nu_{Na\text{-}O}$), 705 $cm^{-1}$ ($\nu_{o\text{–}Na\text{–}o}$), and 516 $cm^{-1}$ ($\nu_{Na\text{–}O} + \nu_{c\text{–}c}$) (Shamsipur et al., 2013).

Furthermore, sodium oxalate can form stronger interactions with both keratin and cellulose. The oxalate ion has two carboxyl groups capable of forming hydrogen bonds with the hydroxyl groups of cellulose. This formation can lead to a membrane coating, which changes its appearance and can affect its permeability. In the case of keratin, which contains various amino acids with functional groups that can interact with oxalate ions, the less soluble sodium oxalate may similarly form a coating, or it could interact more strongly with specific sites on the keratin, leading to changes in its precipitation behavior. Moreover, lyophilized samples displayed WKH on the surface, more prominent in KH precipitated by the strong sulfuric and hydrochloric acids, less in that precipitated by oxalic acids, and almost absent in the KH precipitated by acetic acid and citric acid.

*4.1.2.3.1. ATR-IR of KH obtained from UAH precipitated by different acids.* In the ATR-IR spectra of the KH with varying precipitating acids (Fig. 7), the absorbance bands at 2920 $cm^{-1}$ and 2850 $cm^{-1}$ corresponding to the asymmetric and symmetric stretching vibrations of methylene ($CH_2$) groups change in the cases of sulfuric and oxalic acids, indicating some alteration of cystine structure previously explained. As expected, all bands strongly support the formation of sodium oxalate. Bands around 1320 $cm^{-1}$ ($\nu sym_{(COO-)}$), 778 $cm^{-1}$ ($\delta_{O\text{–}C=O} + \nu_{Na\text{–}O}$), and 516 $cm^{-1}$ ($\nu_{Na\text{–}O} + \nu_{c\text{–}c}$) (Shamsipur et al., 2013; Peterson and Pullman, 2016).

*4.1.2.3.2. TGA and DSC analysis of KH obtained from UAH precipitated by different acids.* In the TGA of KH precipitated using various acids

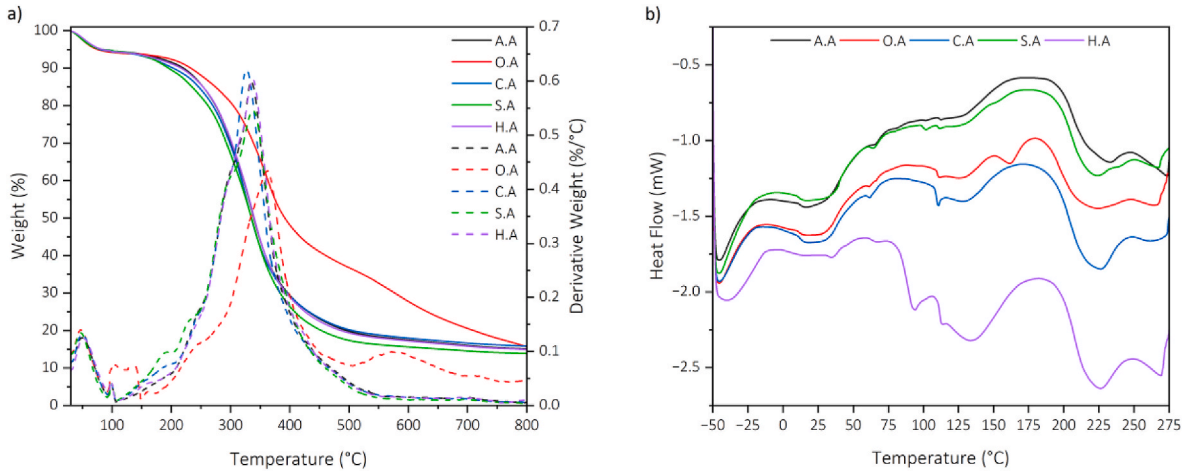


**Fig. 8.** TGA (a) and DSC (b) of KH obtained from UAH precipitated by different acids.

**Table 6**
The effect of different precipitating acids on TAH hydrolysis and KH yield shows variations in process parameters and results. Abbreviations are defined in Table 1.

| NaOH (%) | RF (G) | $V_{Total}$ (mL) | Pre-US pH | A (%) | E (kWh) | T (min) | Post-US pH | T (°C) | Acid used | Acid quantity (g) | RY (g) | AY (%) | WKH |
|---|---|---|---|---|---|---|---|---|---|---|---|---|---|
| 3 | 45 | 450 | 13.69 | 80 | 0.160 | 90 | 13.68 | 75 | Acetic | 32 | 7.56 ± 0.72 | 20.25 ± 1.94 | – |
| 3 | | | 13.76 | | 0.135 | 90 | 13.40 | | Oxalic | 22 | 7.58 ± 1.17 | 20.29 ± 3.14 | + |
| 3 | | | 13.82 | | 0.144 | 90 | 12.65 | | Citric | 25 | 8.54 ± 0.64 | 22.87 ± 1.72 | – |
| 3 | | | 13.70 | | 0.130 | 90 | 12.90 | | Sulfuric (96%) | 20 | 5.17 ± 1.81 | 13.84 ± 4.84 | ++ |
| 3 | | | 13.56 | | 0.134 | 90 | 12.81 | | Hydrochloric (37%) | 36 | 5.15 ± 1.42 | 13.79 ± 3.79 | ++ |

(Fig. 8a), initial weight loss across all samples at approximately 100 °C can be attributed to the desorption of water. For the sample treated with oxalic acid, the weight loss continues steadily up to 150 °C, suggesting the presence of bound water or other volatile components, such as oxalate decomposition products, which may include carbon dioxide and water released from the oxalate ion decomposition. Between 75 °C and 200 °C, the gentle slope of weight loss for the oxalic acid sample indicates a progressive breakdown of sodium oxalate bonds, lattice stretching, and a slow outflow of water molecules (Garcia-Guinea et al., 2011). A plateau observed from around 210 °C–250 °C across the samples may hint at the thermal stability of alpha-helix structures, with the sulfuric acid sample showing a more pronounced thermal event, possibly due to a higher content of these structures or different interactions with the acid used.

As the temperature increases beyond this range, all samples exhibit a sharp decline in weight, reaching a peak decomposition rate between 325 °C and 340 °C. The oxalic acid sample uniquely demonstrates a delayed peak around 362 °C, likely due to the thermal decomposition of sodium oxalate, which can decompose at higher temperatures than pure keratin. This process might involve releasing carbon monoxide and forming sodium carbonate, consistent with the additional weight loss peak at 575 °C (Garcia-Guinea et al., 2011). This peak is absent in other samples, reinforcing the link to sodium oxalate decomposition. Complete keratin degradation is observed at approximately 550 °C for all samples, with the KH precipitated with organic acids leaving a higher carbon residue after thermal degradation. In contrast, the KH precipitated with inorganic acids end with the least residue, possibly due to a more complete breakdown of their constituents.

In the DSC analysis of KH treated with various acids, distinct thermal events corresponding to different keratin decomposition stages and interaction with the acids used are observed (Fig. 8b). The small endothermic peak before 100 °C, notably prominent in the hydrochloric acid-treated sample at 93 °C, at 100 °C, and beyond in the other samples, suggests unbound and bound water desorption. The sulfuric and hydrochloric acid samples exhibit a two-phase water desorption, implying the presence of both loosely bound and more tightly bound water molecules within the sample. Particularly in the oxalic acid-treated sample, a unique endothermic event at 160 °C correlates with similar observations in the TGA analysis, supporting the hypothesis of sodium oxalate bond breakdown. This event is not present in other samples, indicating a distinct behavior due to oxalate presence.

The endothermic peak around 225 °C across all samples is consistent with the melting of alpha-helix structures, a common thermal transition in protein analysis. The intensity of this peak varies, with the hydrochloric acid-treated sample showing the most significant transition, followed by citric, oxalic, sulfuric, and acetic acid-treated samples. This variance in peak intensity could indicate differences in the preservation or decomposition of the alpha-helix structures due to the acidity and strength of the acid used during precipitation. The highest endothermic peak in the hydrochloric acid sample suggests a greater proportion of intact alpha-helices, possibly due to the acid's stronger ionic nature,

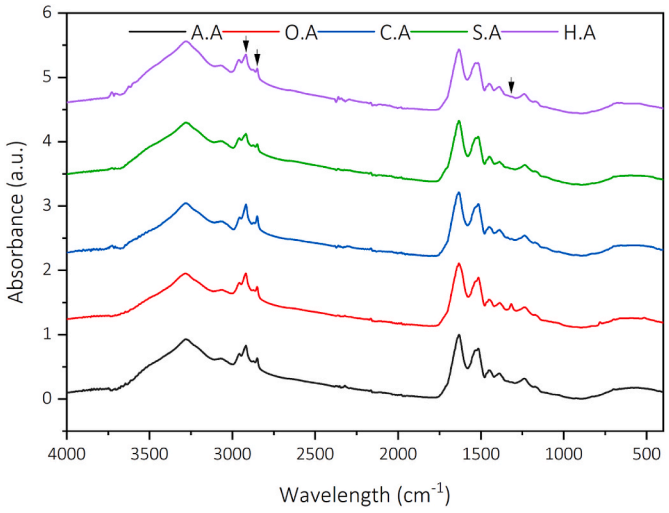


**Fig. 9.** ATR-IR spectra of KH obtained from TAH precipitated by different acids.

which may better stabilize the keratin structure during precipitation. Conversely, the lower intensity in other samples may reflect less alpha-helix content or more disrupted structures, potentially due to the varying interactions between keratin and different acids. The correlation between these endothermic transitions and the corresponding TGA data provides additional insight into the thermal stability and structural integrity of the KH post-precipitation. The data from both analyses contribute to a comprehensive understanding of the effects of acid precipitation on keratin structure and stability, with potential implications for optimizing keratin processing conditions.

#### *4.1.3. Thermal alkaline hydrolysis*

The observed differences in keratin yield between ultrasound-assisted and thermal hydrolysis processes may be attributed to the distinct mechanisms by which heat is generated and distributed within the reaction medium. Ultrasound hydrolysis, characterized by cavitation phenomena, generates localized hot spots due to the collapse of cavitation bubbles, resulting in non-uniform heating and overall heating due to the attenuation of heat transfer within the dense feather biomass inside the reactor. This non-uniformity, coupled with the mechanical effects of ultrasound, may enhance hydrolysis efficiency by effectively disrupting the keratin structure and facilitating the release of soluble proteins without prolonged exposure to heat. In contrast, thermal hydrolysis applies heat directly and uniformly through a heating plate, with continuous stirring. However, this direct and constant heat source, combined with prolonged exposure to heat, may not only be effective in breaking down the keratin but also degrading it, potentially leading to lower yields. In Table 6, the longer duration of TAH at 75 °C for 90 min, compared to 25 min for UAH hydrolysis, further supports this notion, as

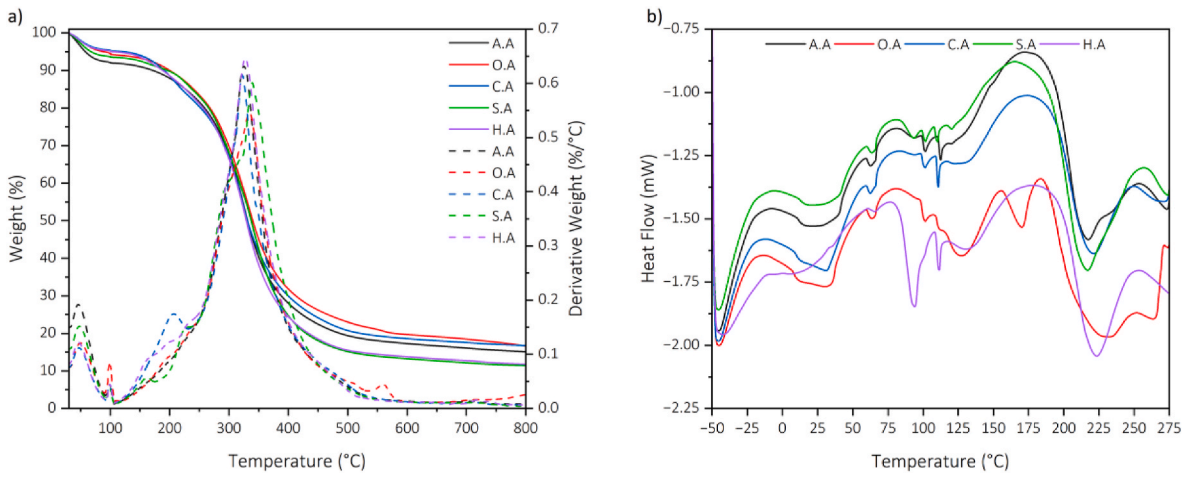


**Fig. 10.** TGA (a) and DSC (b) of KH obtained from TAH precipitated by different acids.

prolonged exposure to heat could result in greater thermal degradation of proteins, thereby reducing the amount of extractable keratin. The stirring introduced during thermal hydrolysis aims to improve heat transfer and mimic the mixing effect of ultrasound. Nevertheless, it appears that the mechanical action of stirring alone is insufficient to match the efficiency of ultrasound's cavitation effect, which exerts additional physical forces that contribute to the disintegration of keratin structures.

*4.1.3.1. ATR-IR of KH obtained from TAH precipitated by different acids.* The ATR-IR spectra of KH obtained from thermal alkaline hydrolysis (Fig. 9) show notable differences in the methylene group region. The bands at 2920 $cm^{-1}$ and 2850 $cm^{-1}$ indicate the asymmetric and symmetric stretching vibrations of methylene ($CH_2$) groups, indicating more keratin structure alteration than UAH. This alteration suggests changes in the protein's structure, possibly due to a longer thermal hydrolysis process affecting the methylene chains within the protein matrix. Similarly to UAH, the bands strongly support sodium oxalate formation in the oxalic acid-precipitated sample. Bands around 1320 $cm^{-1}$ ($\nu sym_{(COO-)}$), 778 $cm^{-1}$ ($\delta_{O-C=O} + \nu_{Na-O}$), and 516 $cm^{-1}$ ($\nu_{Na-O} + \nu_{c-c}$) (Shamsipur et al., 2013; Peterson and Pullman, 2016).

*4.1.3.2. TGA and DSC of KH obtained from TAH precipitated by different acids.* In the TGA of KH obtained with a heating plate (Fig. 10a), the initial weight loss across all samples was around 100 °C, typical of water desorption. Bound water desorption continues until 220 °C for all different KH and is more prominent in the KH precipitated by citric acid. An increase in the decomposition rate in the range of 230 °C–340 °C indicates the thermal stability of the protein structure, similar to that of UAH, with the oxalic acid and sulfuric acid treated samples showing later peak decomposition rates. The complete thermal degradation of keratin is observed at roughly 550 °C for most samples, with a pronounced peak for oxalic-acid treated samples at 560 °C, related to sodium oxalate decomposition. Complete keratin degradation is observed at approximately 550 °C for all samples, with the KH precipitated with organic acids leaving a higher carbon residue after thermal degradation. In contrast, the KH precipitated with inorganic acids end with the least residue, possibly due to a more complete breakdown of their constituents.

In the DSC curves of the KH of TAH precipitated with various acids (Fig. 10b), the small endothermic peaks before 100 °C, in all KH samples and most notable in the KH precipitated with hydrochloric acid, hint at the initial water desorption phase. The sulfuric acid-treated KH shows a more complex desorption pattern, which may indicate the presence of both loosely bound and more structurally integrated water molecules. A unique endothermic event at 170 °C, particularly in the oxalic acid-treated sample, supported the sodium oxalate bond-breakdown hypothesis. The endothermic peak around 215 °C–235 °C across all samples is consistent with the melting of alpha-helix structures. The intensity of this peak varies, with the hydrochloric acid-treated sample showing the most significant transition, followed by oxalic, sulfuric, citric, and acetic acid-treated samples. This variance in peak intensity could indicate differences in the preservation or decomposition of the alpha-helix structures or unfolding of protein secondary structures, such as alpha-helix to beta-sheet transitions, due to the acidity and strength of the acid used during precipitation. The highest endothermic peak in the hydrochloric acid sample suggests a greater proportion of intact alpha-helices, possibly due to the acid's stronger ionic nature, which may better stabilize the keratin structure during precipitation. Conversely, the lower intensity in other samples may reflect less alpha-helix content or more disrupted structures, potentially due to the varying interactions between keratin and different acids.

*4.1.4. Sodium dodecyl sulfate PolyAcrylamide gel electrophoresis (SDS-PAGE) analysis*

The molecular weights of the keratin hydrolysates obtained are presented in Fig. S9a. Lanes 2–4 are the KHs from UAH of NaOH concentrations 1%, 3%, and 5%, respectively, which show a molecular weight of below 10 kDa, with 1% NaOH showing the purest keratin with a well-defined band, whereas the 3% and 5% were accompanied by smearing of the lanes, likely due to fragmented proteins. Lanes (5-6-7-8-9), show KH precipitated by C.A, O.A, A.A, H.A, and S.A, respectively, where all show clean, well-defined bands except that precipitated by oxalic acid, which was accompanied by smearing of the lane, which could be the chelation to sodium oxalate ions, leaving a less pure keratin band (Stock, 2017). (Fig. S9b), Lane 2, showing RF processed through RB, reveals a very pure keratin band, demonstrating that keratin found in feathers is less altered, consistent with Woodin's findings (Woodin, 1954), which suggest feather keratin is predominantly β-keratin. However, the RF processed through UC in Lane 8 shows more altered keratin with more smearing of the lane. Lanes (3–7) are KH of TAH precipitated by C.A, O.A, A.A, H.A, and S.A, respectively. They show more altered keratin than KH in the gel, with KH precipitated by H.A showing the purest keratin with less smearing, consistent with the DSC results before. These results suggest preserving the original keratin structure during alkaline hydrolysis in both UAH and TAH, which also agrees with other studies (Eslahi et al., 2013). The observed keratin hydrolysates with molecular weights around 10 kDa are well-suited for cosmetics, biomedical materials, and biotechnological research due to their enhanced solubility and bioactivity (Tasaki, 2020). These low molecular weight keratins improve hair hydration and skin elasticity in cosmetic products, and their biocompatibility and bioactivity make them ideal for

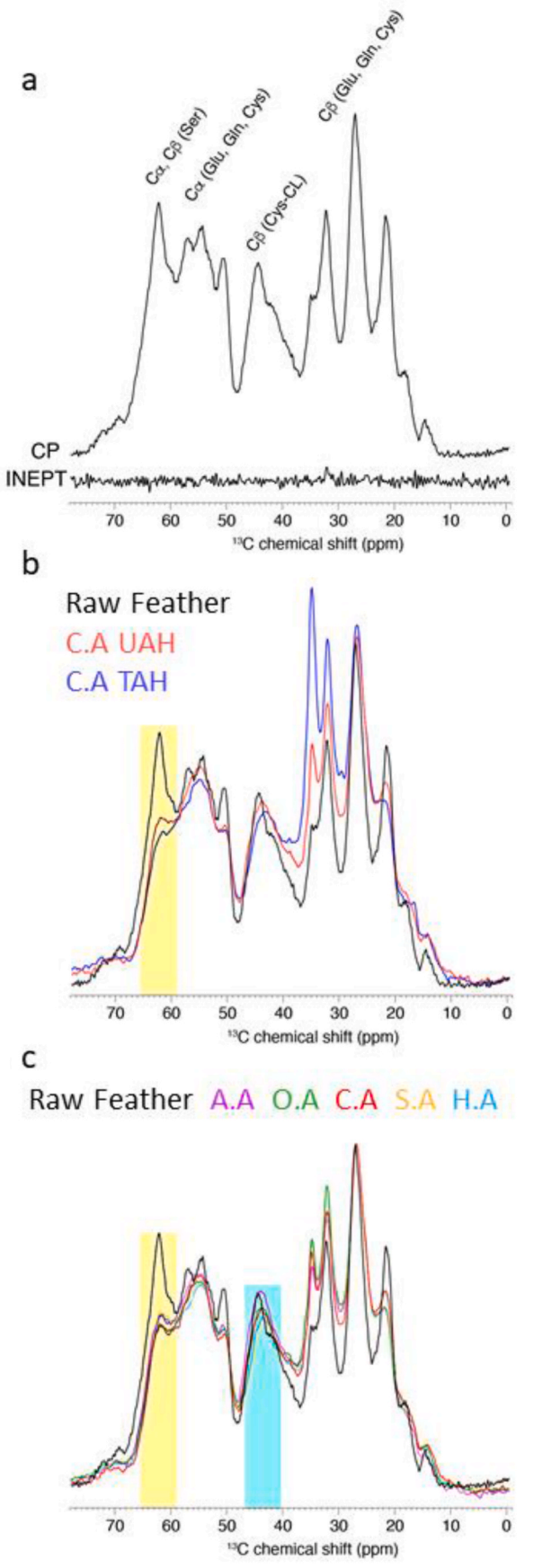


*(caption on next column)*

**Fig. 11.** Solid-state NMR analysis of raw feather and keratin hydrolysates obtained by UAH, TAH, and different precipitating acids. A. $^{13}C$-detected cross-polarization and INEPT spectra of raw feather recorded at 600 MHz at a spinning frequency of 11 kHz. Highlighted in yellow is the chemical shift region of Ser $C^{\beta}$. Comparison of $^{13}C$ CP spectra of raw feather and keratin hydrolysates obtained by UAH and TAH. Comparison of $^{13}C$ CP spectra of raw feather and keratin hydrolysates obtained by UAH using different precipitating acids. Highlighted in yellow is the chemical shift region of Ser $C^{\beta}$.

developing medical hydrogels and dressings for wound healing and skin regeneration (Perța-Crișan et al., 2021).

#### 4.1.5. *Magic-angle spinning solid-state NMR spectroscopy (SSNMR-MAS)*

The proteinaceous nature of keratin filaments makes it a promising target for NMR spectroscopy to investigate structure and conformation at site-specific resolution. Keratin filaments are insoluble and partially heterogeneous, hampering the use of conventional solution NMR. Solid-state NMR offers a powerful technique to study the molecular conformation of keratin filaments (Duer et al., 2003). In this work, cross-polarization (CP) was used as an initial $^{1}H$–$^{13}C$ polarization transfer to reveal the immobile and rigid components of the RF sample. The CP spectrum of RF material leads to a typical $^{13}C$ protein spectral pattern (Fig. 11a). Keratin mainly comprises Glu, Gln, Cys, and Ser residues, representing ~50% of total amino acids. There were unambiguously identified signals belonging to Ser $^{13}C^{\beta}$ based on their characteristic chemical shift values, ranging between 65 and 69 ppm (referred to DSS), using reported database values (Wang and Jardetzky, 2002). $^{13}C^{\alpha}$ chemical shifts for Glu and Gln appear at 54–59 ppm depending on their secondary structure. SSNMR provides a reliable probe to distinguish between free and disulfide-bonded cysteines (Sharma and Rajarathnam, 2000) because their $^{13}C^{\beta}$ chemical shifts are very sensitive to oxidation. Here, the spectral region at ~40–43 ppm contains $C^{\beta}$ contribution from cross-linked Cys, with free cysteine having $C^{\beta}$ at ~27–29.5 ppm. In addition to CP, a $^{13}C$ experiment was recorded using an INEPT polarization transfer (Fig. 11a) with no detectable signals, indicating the absence of highly mobile molecular species in the keratin sample. A comparison of CP $^{13}C$ spectral patterns obtained on extracted keratin using these two conditions with a citric acid treatment at 75 °C was done to investigate the effect of ultrasound *versus* thermal alkaline hydrolysis. Resulting SSNMR spectra showed that the overall keratin spectral pattern observed for the RF sample is conserved, indicative no major changes in the keratin protein composition. It can be observed, for both UAH and TAH, broader NMR lines compared to RF. This loss of spectral resolution in CP experiments strongly suggests that the static structural disorder is increased after UAH and TAH treatments, possibly due to the breaking of disulfide bonds.

In the spectral analysis on the region at ~60–65 ppm (highlighted in yellow, Fig. 11b), which primarily encodes for $C^{\beta}$ resonances of Ser. A clear shift of the signals can be observed when comparing UAH and TAH treatments to RF, with a loss of signal for both treatments (Fig. 11b) at 60–63 ppm. This loss reflects a change in the secondary structure, with a decrease in residues involved in α-helical secondary structure elements (Wang and Jardetzky, 2002). As a hypothesis, considering results obtained with ATR-IR, TGA, and DSC analysis disrupting cross-linked cysteines in α-helices might lead to more amino acid content in β-sheet and random coil secondary structural elements. This observation is corroborated by the broader lines observed after UAH and TAH treatments, indicative of a loss of structural stability (i.e., unrestricted movement) and the subsequent formation of a more heterogeneous β-sheet or extended structure after the treatments.

The $^{13}C$ spectral patterns of keratin treated with citric, oxalic, acetic, sulfuric, and hydrochloric acids at 75 °C (Fig. 11c) were compared to document the effect of various organic acids combined with ultrasound. All acid treatments led to a partial loss of spectral resolution, encoded in the $^{13}C$ line widths, indicative of a less ordered keratin structure. Among the different acids, we identified citric acid as less efficient in altering

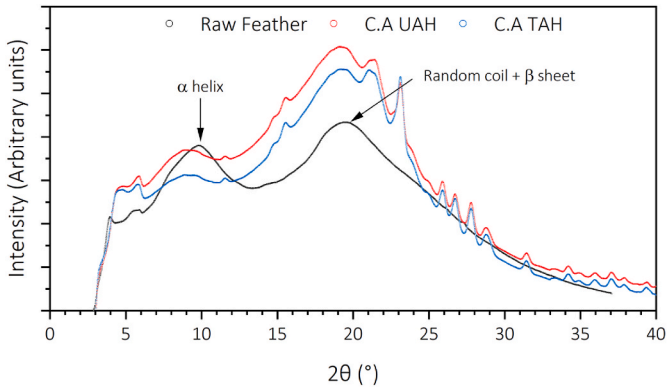


**Fig. 12.** Comparison of XRD patterns of raw feather (black), keratin hydrolysate obtained by UAH using citric acid, 10:100 (blue) and keratin hydrolysate obtained by TAH using citric acid at 75 °C, and 10:100 (red).

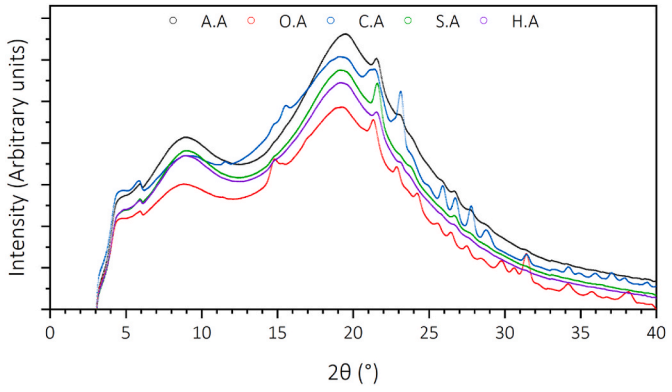


**Fig. 13.** Comparison of XRD patterns of raw feather (black) and keratin extracted after ultrasound extractions using various acids at 75 °C.

the overall structural order of keratin filaments. Next, the effect of these organic acids and their ability to disrupt -S-S- disulfide links associated with cysteine residues were compared. It can be observed that the loss of signal at ~40–43 ppm (highlighted in cyan in Fig. 11c), indicative of cross-linked cysteine, is influenced by the nature of the organic acid used for the treatment. It can be observed that the relative abundance of cross-linked cysteine is less impacted when feathers are treated with acetic acid, while sulfuric and hydrochloric acids induce the most crucial effect. In line with TGA and DSC results, the proper choice of acidity and strength of the acids used during the treatment could potentially tune and optimize the structural perturbation of keratin.

#### *4.1.6. X-ray diffraction (XRD)*

X-ray diffraction experiment (XRD) was performed on a raw leather sample to confirm, as expected from previous studies (Alvarez et al., 2023), the semi-crystalline state of the molecular structure (Fig. 12). The diffraction patterns result from the contribution of three types of crystal diffraction peaks: the meridional reflections (2θ between 15° and 31°) for α-helix structure, the equatorial reflections (2θ between 16° and 31°) for random coil and β-sheet structures and the equatorial reflections (2θ = 9°) for α-helix and β-sheet structures. Due to the overlapping signals at about 18° and 19° from the α-helix and β-sheet, both are unable to be unambiguously assigned. The comparison of X-ray diffraction patterns (XRD) of raw feather, keratin obtained by UAH, and TAH are shown in Fig. 12 confirmed, as expected, that the feather and keratin hydrolysate are mainly composed of β-sheet and random coil conformations. The combined UAH, TAH, and different acidic treatments (Fig. 12) show the largest decrease in the peak intensity related to α helix contribution and is consistent with the CP MAS NMR spectra (vide infra).

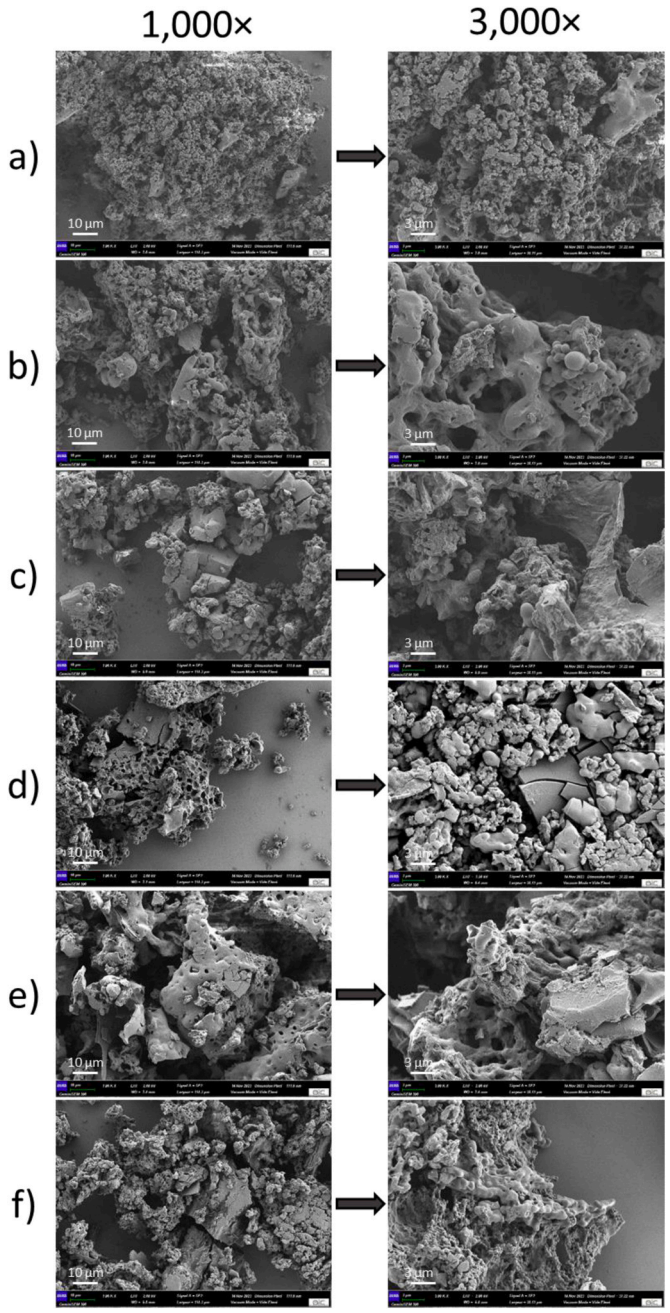


**Fig. 14.** SEM images of a) acetic, b) oxalic, c) citric, d) sulfuric, e) hydrochloric, f) TAH-citric.

The overall comparison of keratin extracted after UAH using different acids (Fig. 13) shows a decrease in diffraction peak intensities around 9° and an enlargement of the peaks at about 19°, which is directly related to the disruption of the α-helix structures and more precisely to the disulfide bonds breakage. Minor shifting between the peaks in our samples may indicate some differences between the crystalline domains of the keratin. Diffraction peaks at higher 2θ values might be assigned to salt crystals formed after the acidic treatment.

#### *4.1.7. Scanning electron microscopy (SEM)*

The surface morphology of different KH precipitated with different acids was explored by SEM analysis. The SEM images for the KH are shown in Fig. 14. SEM images revealed that the keratin powder showed different morphologies according to the acid used for precipitation. In this case, KH precipitated by citric and acetic acids showed microspheres

of different diameter ranges. These spheres were more relevant in the KH precipitated with citric acid in both UAH and TAH. A similar morphology was observed in previous reports for feather and wool keratin particles (Sharma et al., 2018; Yin et al., 2013; Zhang et al., 2013). Weaker acids might cause less disruption to the hydrophobic and hydrophilic balance in the proteins, allowing more controlled precipitation, so they reorganize or fold into energetically favorable structures, such as spheres.

On the other hand, keratin treated with oxalic acid showed more dust-like structures or small aggregates. In addition to this, the KH precipitated by oxalic acid showed crystallites with different morphologies and sizes of sodium oxalate faces that have been incorporated into the keratin, shown in Fig. S10; these were similar to images of sodium oxalates in prior studies [54]. The presence of these oxalates might explain the different structures obtained, which may be due to the chelation effect of oxalic acid and sodium occurring simultaneously and reducing free oxalic acid ions in the medium. This phenomenon could lead to a less controlled precipitation process. Instead of forming organized structures like spheres, the keratin might aggregate in a less ordered manner, leading to dust-like particles.

KH precipitated with the stronger acids sulfuric or hydrochloric, showing randomly arranged porous microstructures. This arrangement could be due to the more drastic pH changes when these acids are added, leading to more extensive denaturation and unfolding of the protein chains. The unfolding can expose more hydrophobic regions, leading to irregular aggregations and interactions, possibly resulting in more porous structures than well-defined spheres. Although feathers initially showed microfibers and honeycomb structures (Fig. S11), the surface structure of the residue changed significantly after ultrasound-assisted alkaline hydrolysis. The reason is that ultrasound-assisted technology aggravates the damage of the cell wall. In the ultrasonic treatment process, the cavitation effect, mechanical effect, and thermal effect of the ultrasonic wave act on the cell wall together, causing the destruction and collapse of the network structure of the cell wall, increasing the contact area between the solvent and the residue, thus promoting the release of keratin (Zhong et al., 2022). Unlike ultrasound, thermal hydrolysis does not involve the same level of mechanical disruption, meaning that the keratin structures are likelier to break down into smaller particles than large agglomerates. Moreover, due to the longer duration and lower intensity of thermal hydrolysis, the keratin proteins have more time to unfold and re-aggregate in a controlled manner. This timelapse can result in smaller, more tightly packed aggregates than the less packed and irregular agglomerates formed through ultrasound hydrolysis.

## 5. Conclusion

This study investigates how factors such as particle size, alkali concentration, liquid-to-solid ratio, reactor geometry, precipitation temperature, pH, and precipitating acid affect the yield and quality of keratin hydrolysates. Exploring these factors was crucial for enhancing understanding of the intricate mechanisms governing feather hydrolysis and keratin recovery, a field where reproducibility is a considerable challenge. The findings reveal that UAH surpasses TAH in terms of yield and preserving the main structure of keratin. Optimal conditions identified for UAH were 3% NaOH, an L/S ratio of 100:10 in a cylindrical vessel, and ultrasonic energy of 100 Wh/L at a frequency of 26 kHz, using citric acid at pH 4.5 for low-temperature precipitation. Specifically, UAH achieved a 70% yield within 25 min, leveraging the localized high temperatures and pressures of cavitation phenomena. This method efficiently disrupted the keratin structure and facilitated the release of soluble proteins without leading to their degradation, as confirmed by ATR-IR and gel-electrophoresis.

Conversely, TAH, required 90 min to reach just a 23% yield, with the extended heat exposure contributing to the thermal degradation of keratin. TGA analysis revealed that keratin decomposition occurs between 200 and 550 °C. XRD and NMR analyses indicated that post-hydrolysis, across both UAH and TAH, keratin primarily consists of β-sheet and random coil structures, with a reduction in α-helix content and a less ordered structure compared to raw feather, likely due to disulfide bridge cleavage in cystine. Different acids used for precipitation affected the keratin structure differently, with citric acid showing the least impact, while acetic acid best-preserved cystine linkages, outperforming sulfuric and hydrochloric acids. These results highlight that the proper choice of treatment parameters can fine-tune and optimize the structural perturbation of keratin. Moreover, they highlight the potential of ultrasound-assisted alkaline hydrolysis as an eco-friendly and economical method for managing keratinous waste and enhancing keratin recovery.

## CRediT authorship contribution statement

**Nidal Del Valle Raydan:** Writing – original draft, Methodology, Investigation, Data curation, Conceptualization. **Antoine Loquet:** Writing – review & editing, Formal analysis. **Birgit Habenstein:** Writing – original draft, Formal analysis. **Brice Kauffmann:** Writing – original draft, Formal analysis. **Bertrand Charrier:** Validation, Supervision, Resources. **Gregory Chatel:** Writing – review & editing, Supervision, Conceptualization. **Eduardo Robles:** Writing – review & editing, Data curation, Conceptualization.

## Declaration of competing interest

The authors declare the following financial interests/personal relationships which may be considered as potential competing interests: Eduardo Robles reports financial support was provided by French National Research Agency. Nidal Del Valle Raydan reports financial support was provided by Nouvelle-Aquitaine Regional Council. If there are other authors, they declare that they have no known competing financial interests or personal relationships that could have appeared to influence the work reported in this paper.

## Data availability

Data will be made available on request.

## Acknowledgements

ER. Was supported by the Agence Nationale de la Recherche (ANR-16-IDEX-0002); N.R. got funding from the Conseil Régional Aquitaine (AAPR2020-8631210). Research mobility of N.R. to EDYTEM, Chambery was funded by ReUNITA. This work has benefited from the Biophysical and Structural Chemistry Platform at IECB, CNRS UAR 3033, INSERM US001.

## Appendix A. Supplementary data

Supplementary data to this article can be found online at https://doi.org/10.1016/j.jclepro.2024.142927.

## References

Alvarez, S., Raydan, N.D.V., Svahn, I., Gontier, E., Rischka, K., Charrier, B., Robles, E., 2023. Assessment and characterization of duck feathers as potential source of Biopolymers from an upcycling perspective, 2023 Sustain. Times 15. https://doi.org/10.3390/SU151914201. Page 14201 15, 14201.

Bhavsar, P., Zoccola, M., Patrucco, A., Montarsolo, A., Rovero, G., Tonin, C., 2017. Comparative study on the effects of superheated water and high temperature alkaline hydrolysis on wool keratin. Textil. Res. J. 87, 1696–1705. https://doi.org/10.1177/0040517516658512.

Boga, C., Taddei, P., Micheletti, G., Ascari, F., Ballarin, B., Morigi, M., Galli, S., 2014. Formaldehyde replacement with glyoxylic acid in semipermanent hair straightening: a new and multidisciplinary investigation. Int. J. Cosmet. Sci. 36, 459–470. https://doi.org/10.1111/ics.12148.

Bragulla, H.H., Homberger, D.G., 2009. Structure and functions of keratin proteins in simple, stratified, keratinized and cornified epithelia. J. Anat. 214, 516–559. https://doi.org/10.1111/j.1469-7580.2009.01066.x.
Burnett, C.L., Bergfeld, W.F., Belsito, D.V., Hill, R.A., Klaassen, C.D., Liebler, D.C., Marks, J.G., Shank, R.C., Slaga, T.J., Snyder, P.W., Gill, L.J., Heldreth, B., 2021. Safety assessment of keratin and keratin-derived ingredients as used in cosmetics. Int. J. Toxicol. 40, 36S–51S. https://doi.org/10.1177/10915818211013019.
Bussemaker, M., 2013. Parametric Influences of Ultrasound in Homogeneous and Heterogeneous Mixtures for Biofuel and Biorefinery Applications. University of Western Australia.
Calinescu, I., Vartolomei, A., Gavrila, I.A., Vinatoru, M., Mason, T.J., 2019. A reactor designed for the ultrasonic stimulation of enzymatic esterification. Ultrason. Sonochem. 54, 32–38. https://doi.org/10.1016/j.ultsonch.2019.02.018.
Callegaro, K., Brandelli, A., Daroit, D.J., 2019. Beyond plucking: feathers bioprocessing into valuable protein hydrolysates. Waste Manag. 95, 399–415. https://doi.org/10.1016/j.wasman.2019.06.040.
Chen, H., Gao, S., Li, Y., Xu, H.J., Li, W., Wang, J., Zhang, Y., 2022. Valorization of livestock keratin waste: application in agricultural fields. Int. J. Environ. Res. Publ. Health 19. https://doi.org/10.3390/ijerph19116681.
Chen, P.Y., McKittrick, J., Meyers, M.A., 2012. Biological materials: functional adaptations and bioinspired designs. Prog. Mater. Sci. 57, 1492–1704. https://doi.org/10.1016/j.pmatsci.2012.03.001.
Chen, Y., Huang, Y., Chen, X., 2013. Acoustic propagation in viscous fluid with uniform flow and a novel design methodology for ultrasonic flow meter. Ultrasonics 53, 595–606. https://doi.org/10.1016/j.ultras.2012.10.005.
Chilakamarry, C.R., Mahmood, S., Saffe, S.N.B.M., Arifin, M.A. Bin, Gupta, A., Sikkandar, M.Y., Begum, S.S., Narasaiah, B., 2021. Extraction and application of keratin from natural resources: a review. 3 Biotech 11, 1–12. https://doi.org/10.1007/S13205-021-02734-7/FIGURES/7.
Coward-Kelly, G., Chang, V.S., Agbogbo, F.K., Holtzapple, M.T., 2006. Lime treatment of keratinous materials for the generation of highly digestible animal feed: 1. Chicken feathers. Bioresour. Technol. 97, 1337–1343. https://doi.org/10.1016/j.biortech.2005.05.021.
Duer, M.J., McDougal, N., Murray, R.C., 2003. A solid-state NMR study of the structure and molecular mobility of α-keratin. Phys. Chem. Chem. Phys. 5, 2894–2899. https://doi.org/10.1039/b302506c.
Dzah, C.S., Dzigbor, A., 2023. Ultrasound assisted extraction: a relook at solvent to material ratio, its effects on process efficiency and how it can be exploited for different uses. J. Food Process. Eng. 46, 1–13. https://doi.org/10.1111/jfpe.14339.
Eslahi, N., Dadashian, F., Nejad, N.H., 2013. An investigation on keratin extraction from wool and feather waste by enzymatic hydrolysis. Prep. Biochem. Biotechnol. 43, 624–648. https://doi.org/10.1080/10826068.2013.763826.
European Commission, n.d. Information on an overview of EU poultry, market measures and standards, trade measures, market monitoring, legal bases and committees. [WWW Document]. Agric. Rural Dev.
Eurostat, 2023. Agricultural Production - Livestock and Meat.
Expert Group for Agricultural Markets, 2023. EU Market Situation for Poultry.
Farrelly & Mitchell, 2023. Unlocking a feather bioeconomy for keratin-based agricultural products. https://doi.org/10.3030/101023306.
Feroz, S., Muhammad, N., Dias, G., Alsaiari, M.A., 2022. Extraction of keratin from sheep wool fibres using aqueous ionic liquids assisted probe sonication technology. J. Mol. Liq. 350, 118595 https://doi.org/10.1016/j.molliq.2022.118595.
Fung, B.M., Khitrin, A.K., Ermolaev, K., 2000. An improved broadband decoupling sequence for liquid crystals and solids. J. Magn. Reson. 142, 97–101. https://doi.org/10.1006/jmre.1999.1896.
Garcia-Guinea, J., Correcher, V., Lozano-Diz, E., Bañares, M.A., Lopez-Arce, P., García, A. M., Moreno, D.A., 2011. Effect of thermal annealing on synthetic sodium oxalate crystals. J. Anal. Appl. Pyrolysis 91, 332–337. https://doi.org/10.1016/j.jaap.2011.03.011.
Grazziotin, A., Pimentel, F.A., De Jong, E.V., Brandelli, A., 2006. Nutritional improvement of feather protein by treatment with microbial keratinase. Anim. Feed Sci. Technol. 126, 135–144. https://doi.org/10.1016/j.anifeedsci.2005.06.002.
Helmick, H., Ettestad, S., Kokini, J.L., 2023. Estimation of cold denaturation temperature and its utilization in predicting protein stability as an aid in functionalizing pea protein isolate through cold denaturation. Innovat. Food Sci. Emerg. Technol. 89, 103479 https://doi.org/10.1016/j.ifset.2023.103479.
Holkar, C.R., Jadhav, A.J., Bhavsar, P.S., Kannan, S., Pinjari, D.V., Pandit, A.B., 2016. Acoustic cavitation assisted alkaline hydrolysis of wool based keratins to produce organic amendment fertilizers. ACS Sustain. Chem. Eng. 4, 2789–2796. https://doi.org/10.1021/acssuschemeng.6b00298.
Hong, C., Zhu, J.Q., Zhao, Y.M., Ma, H., 2022. Effects of dual-frequency slit ultrasound on the enzymolysis of high-concentration hydrolyzed feather meal: biological activities and structural characteristics of hydrolysates. Ultrason. Sonochem. 89, 106135 https://doi.org/10.1016/j.ultsonch.2022.106135.
Hoo, D.Y., Low, Z.L., Low, D.Y.S., Tang, S.Y., Manickam, S., Tan, K.W., Ban, Z.H., 2022. Ultrasonic cavitation: an effective cleaner and greener intensification technology in the extraction and surface modification of nanocellulose. Ultrason. Sonochem. 90, 106176 https://doi.org/10.1016/j.ultsonch.2022.106176.
Ji, Y., Chen, J., Lv, J., Li, Z., Xing, L., Ding, S., 2014. Extraction of keratin with ionic liquids from poultry feather. Sep. Purif. Technol. 132, 577–583. https://doi.org/10.1016/j.seppur.2014.05.049.
Jonas, J., 1997. Cold denaturation of proteins. ACS Symp. Ser. 676, 310–323. https://doi.org/10.1021/bk-1997-0676.ch022.
Kshetri, P., Singh, P.L., Chanu, S.B., Singh, T.S., Rajiv, C., Tamreihao, K., Singh, H.N., Chongtham, T., Devi, A.K., Sharma, S.K., Chongtham, S., Singh, M.N., Devi, Y.P., Devi, H.S., Roy, S.S., 2022. Biological activity of peptides isolated from feather keratin waste through microbial and enzymatic hydrolysis. Electron. J. Biotechnol. 60, 11–18. https://doi.org/10.1016/j.ejbt.2022.08.001.
Laemmli, U.K., 1970. Cleavage of structural proteins during the assembly of the head of bacteriophage T4. Nature 227, 680–685. https://doi.org/10.1038/227680a0.
Mokrejs, P., Hutta, M., Pavlackova, J., Egner, P., Benicek, L., 2017. The cosmetic and dermatological potential of keratin hydrolysate. J. Cosmet. Dermatol. 16, e21–e27. https://doi.org/10.1111/jocd.12319.
Mondal, J., Lakkaraju, R., Ghosh, P., Ashokkumar, M., 2021. Acoustic cavitation-induced shear: a mini-review. Biophys. Rev. 13, 1229–1243.
Pan, F., Xiao, Y., Zhang, L., Zhou, J., Wang, C., Lin, W., 2023. Leather wastes into high-value chemicals: keratin-based retanning agents via UV-initiated polymerization. J. Clean. Prod. 383, 135492 https://doi.org/10.1016/j.jclepro.2022.135492.
Papadopoulos, M.C., 1985. Amino acid content and protein solubility of feather meal as affected by different processing conditions. Neth. J. Agric. Sci. 33, 317–319. https://doi.org/10.18174/njas.v33i3.16849.
Pedrosa, N. de A., de Andrade, C.J., Petrus, J.C.C., Monteiro, A.R., 2022. Sequential hydrolysis of chicken feathers composed of ultrasound and enzymatic steps: an enhanced protein source with bioactive peptides. Biomass 2, 237–249. https://doi.org/10.3390/biomass2040016.
Perța-Crișan, S., Ursachi, C. Ștefan, Gavrilaș, S., Oancea, F., Munteanu, F.D., 2021. Closing the loop with keratin-rich fibrous materials. Polymers 13, 1–26. https://doi.org/10.3390/polym13111896.
Peterson, K.I., Pullman, D.P., 2016. Determining the structure of oxalate anion using infrared and Raman spectroscopy coupled with Gaussian calculations. J. Chem. Educ. 93, 1130–1133. https://doi.org/10.1021/acs.jchemed.6b00118.
Qiu, J., Wilkens, C., Barrett, K., Meyer, A.S., 2020. Microbial enzymes catalyzing keratin degradation: classification, structure, function. Biotechnol. Adv. 44, 107607 https://doi.org/10.1016/J.BIOTECHADV.2020.107607.
Riesz, P., Berdahl, D., Christman, C.L., 1985. Free radical generation by ultrasound in aqueous and nonaqueous solutions. Environ. Health Perspect. 64, 233–252. https://doi.org/10.1289/ehp.8564233.
Sarma, A., 2022. Biological importance and pharmaceutical significance of keratin: a review. Int. J. Biol. Macromol. 219, 395–413. https://doi.org/10.1016/j.ijbiomac.2022.08.002.
Shamsipur, M., Roushani, M., Pourmortazavi, S.M., 2013. Electrochemical synthesis and characterization of zinc oxalate nanoparticles. Mater. Res. Bull. 48, 1275–1280. https://doi.org/10.1016/j.materresbull.2012.12.032.
Sharma, D., Rajarathnam, K., 2000. 13C NMR chemical shifts can predict disulfide bond formation. J. Biomol. NMR 18, 165–171. https://doi.org/10.1023/A:1008398416292.
Sharma, S., Gupta, A., Kumar, A., Kee, C.G., Kamyab, H., Saufi, S.M., 2018. An efficient conversion of waste feather keratin into ecofriendly bioplastic film. Clean Technol. Environ. Policy. https://doi.org/10.1007/s10098-018-1498-2.
Shavandi, A., Bekhit, A.E.D.A., Carne, A., Bekhit, A., 2017. Evaluation of keratin extraction from wool by chemical methods for bio-polymer application. J. Bioact. Compat Polym. 32, 163–177. https://doi.org/10.1177/0883911516662069.
Shi, Z., Olson, C.A., Bell, A.J., Kallenbach, N.R., 2001. Stabilization of α-helix structure by polar side-chain interactions: complex salt bridges, cation-π interactions, and C-H···O H-bonds. Biopolym. - Pept. Sci. Sect. 60, 366–380. https://doi.org/10.1002/1097-0282(2001)60:5<366::AID-BIP10177>3.0.CO;2-5.
Sigma Aldrich, 2024. Solubility table of compounds in water at temperature [WWW Document]. https://www.sigmaaldrich.com/FR/fr/support/calculators-and-apps/solubility-table-compounds-water-temperature, 5.9.24.
Staroń, P., Banach, M., Kowalski, Z., Staroń, A., 2014. Hydrolysis of keratin materials derived from poultry industry. Proc. ECOpole 8, 443–448. https://doi.org/10.2429/proc.2014.8(2)050.
Stock, A., 2017. Analysis of methods for extracting matrix proteins from human kidney stones. Urol. Nephrol. Open Access J 4. https://doi.org/10.15406/unoaj.2017.04.00111.
Tasaki, K., 2020. A novel thermal hydrolysis process for extraction of keratin from hog hair for commercial applications. Waste Manag. 104, 33–41. https://doi.org/10.1016/j.wasman.2019.12.042.
Turner, M.D., Sapp, J., 2023. Fire and brimstone: SO2 as a chemical weapon in history. Mil. Med. 188, 286–288. https://doi.org/10.1093/milmed/usad160.
Wang, W., Nema, S., Teagarden, D., 2010. Protein aggregation-Pathways and influencing factors. Int. J. Pharm. 390, 89–99. https://doi.org/10.1016/j.ijpharm.2010.02.025.
Wang, Y., Jardetzky, O., 2002. Probability-based protein secondary structure identification using combined NMR chemical-shift data. Protein Sci. 11, 852–861. https://doi.org/10.1110/ps.3180102.
Woodin, A.M., 1954. Molecular size, shape and aggregation of soluble feather keratin. Biochem. J. 57, 99–109. https://doi.org/10.1042/bj0570099.
Yazdanparast, R., Esmaeili, M.A., Khodagholi, F., 2007. Control of aggregation in protein refolding: cooperative effects of artificial chaperone and cold temperature. Int. J. Biol. Macromol. 40, 126–133. https://doi.org/10.1016/j.ijbiomac.2006.06.018.
Yimer, T.T., 2017. Valorisation of Waste Chicken Feathers: Production of Hoigh-Value Materials. University of KwaZulu-Natal.
Yin, X.C., Li, F.Y., He, Y.F., Wang, Y., Wang, R.M., 2013. Study on effective extraction of chicken feather keratins and their films for controlling drug release. Biomater. Sci. 1, 528–536. https://doi.org/10.1039/c3bm00158j.
Zhang, J., Li, Y., Li, J., Zhao, Z., Liu, X., Li, Z., Han, Y., Hu, J., Chen, A., 2013. Isolation and characterization of biofunctional keratin particles extracted from wool wastes. Powder Technol. 246, 356–362. https://doi.org/10.1016/j.powtec.2013.05.037.

Zhang, Y., Zhao, W., Yang, R., 2015. Steam flash explosion assisted dissolution of keratin from feathers. ACS Sustain. Chem. Eng. https://doi.org/10.1021/acssuschemeng.5b00310.

Zhong, X., Zhang, S., Wang, H., Yang, J., Li, L., Zhu, J., Liu, Y., 2022. Ultrasound-alkaline combined extraction improves the release of bound polyphenols from pitahaya (Hylocereus undatus 'Foo-Lon') peel: composition, antioxidant activities and enzyme inhibitory activity. Ultrason. Sonochem. 90, 106213 https://doi.org/10.1016/j.ultsonch.2022.106213.

Zoccola, M., Aluigi, A., Patrucco, A., Vineis, C., Forlini, F., Locatelli, P., Sacchi, M.C., Tonin, C., 2012. Microwave-assisted chemical-free hydrolysis of wool keratin. Textil. Res. J. 82, 2006–2018. https://doi.org/10.1177/0040517512452948.